Fragility Analysis on the Seismic Response of Freestanding Equipment

Giorgio Lupoi

Ph.D. Student
European School for Advanced Studies in Reduction of Seismic Risk, Rose School
University of Pavia

Dimitrios Konstantinidis

Ph.D. Student
Department of Civil and Environmental Engineering
University of California, Berkeley

Nicos Makris

Professor
Department of Civil and Environmental Engineering
University of California, Berkeley

Abstract

……

……

……

……

Contents

List of Figures

List of Tables

1 Introduction

During strong earthquake shaking heavy equipment located at various floor levels of hospital, laboratories and other critical facilities might slide appreciably, rock or even overturn. Recently, the University of California supported on in-dept study on the seismic response of building contents that range from low-temperature refrigerators and heavy incubators to lighter computer equipment located on desks and shelves.

The study reported in this paper concentrates on the fragility analysis of freestanding equipment located at various levels of a U.C. Berkeley Science Laboratory building. In this work we have investigated the sliding problem, relating the maximum displacement (demand) to two different Intensity Measures (*IM*). The first intensity measure involves only the peak table acceleration (*PTA*) while the second intensity measure requires more detailed information of the seismic input motion—that is the amplitude and the duration of the most distinguishable acceleration pulse.

2 Seismic Hazard

This work is a part of a wider study on the seismic response analysis of the contents of a laboratory on the main campus of U.C. Berkeley. (Reference ???)

The seismic hazard on the Berkeley campus is dominated by potential ground motions generated from the Hayward fault which is located less than one kilometer east of the central campus. The Hayward fault is a strike-slip fault that has a potential to generate earthquakes having magnitudes as large as $M_W = 7.0$. For a hazard level equal to 50% in 50 years the largest contributions come from earthquakes in the magnitude range of $M_W = 5.5$ to 6.0. For hazard level equal to 10% in 50 years and to 2% in 50 years the largest contributions come from earthquakes in the magnitude range of $M_W = 6.5$ to 7.0. The motion listed in Table 2-1 have been selected to satisfy (to the extent possible) the magnitude and the distance combination from a strike-slip earthquake on S_C soil type (Somerville 2001).

Table 2-1: List of the selected records

Earthquake	**Record**	**M_w**	**Distance** [km]	**Hazard Level**
Aigion, Greece (Ground) June 15, 1995	OTE, FP	6.2	5.0	-
Coyote Lake, California (Ground) August 06, 1979	Gilroy Array #6, FN	5.7	3.0	-
Parkfield, California (Ground and 6th floor) June 27, 1966	Cholome Array #8, FN	6.0	8.0	50% in 50yrs
Coyote, California (Ground and 6th floor) August 06, 1979	Gilroy Array #6, FN	5.7	3.0	50% in 50yrs
Loma Prieta (Ground and 6th floor) October 17, 1989	Gavilan College, FN	7.0	9.5	10% in 50yrs
Tottori, Japan (Ground and 6th floor) October 06, 2000	Kofu, FN	6.6	10.0	10% in 50yrs

The interest of the U.C. Berkeley administration on the seismic response of the U.C. lab building has supported a comprehensive nonlinear dynamic analysis of the building which resulted in

simulated floor motions. Floor motions are of unique interest in assessing the seismic response of building contents since they differ appreciably from ground motions.

Figure 2-1 (left) plots four ground motions used in this study, while figure 2-1 (right) plots the corresponding 6^{th} floor motions of the U.C. Berkeley Lab building.

Floor motions impose larger base displacements than the associated ground motions and their frequency content is more concentrated around the first natural frequency of the building.

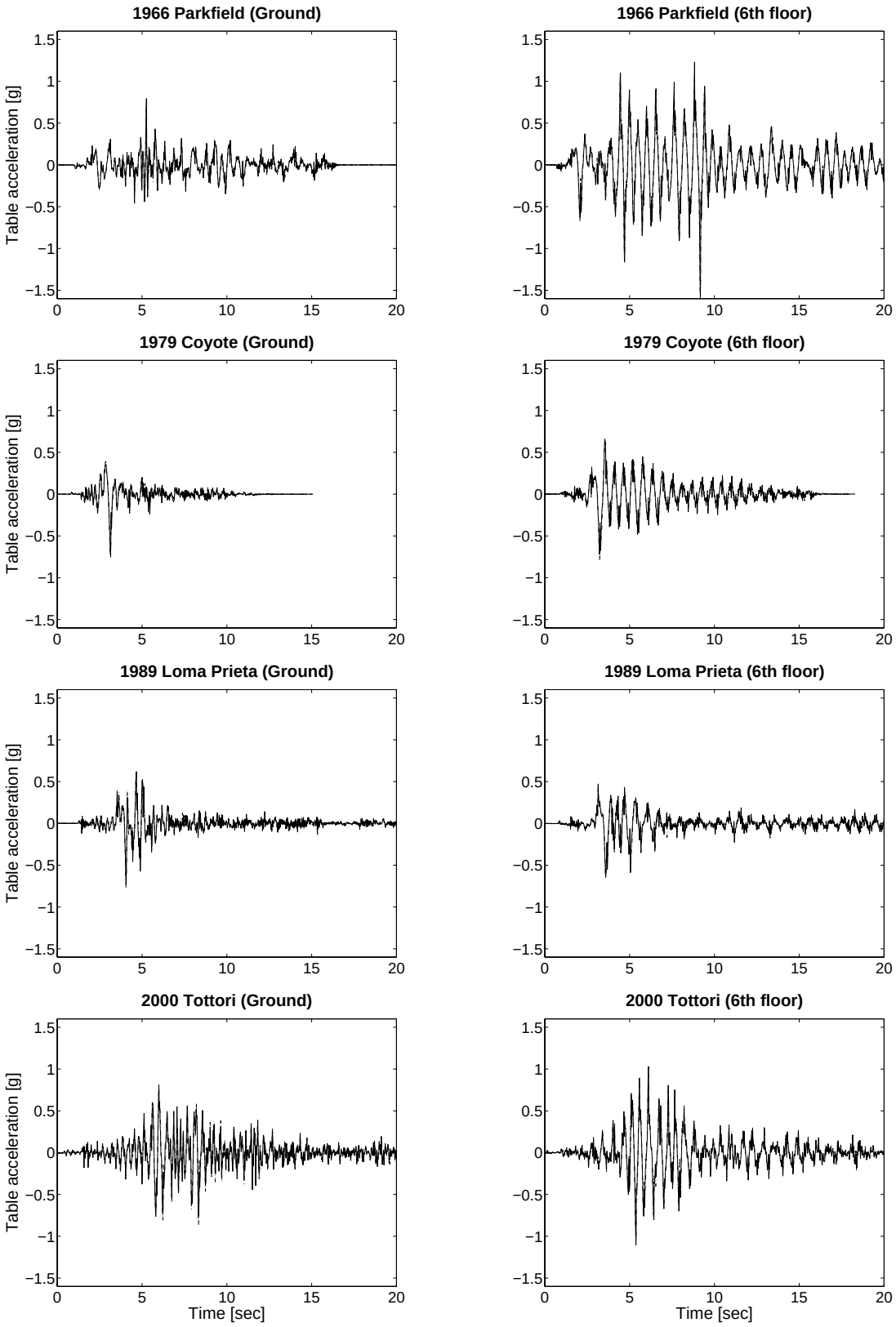

Figure 2-1: Acceleration time histories of four ground motions used in this study (left) together with the resulting 6th floor motions

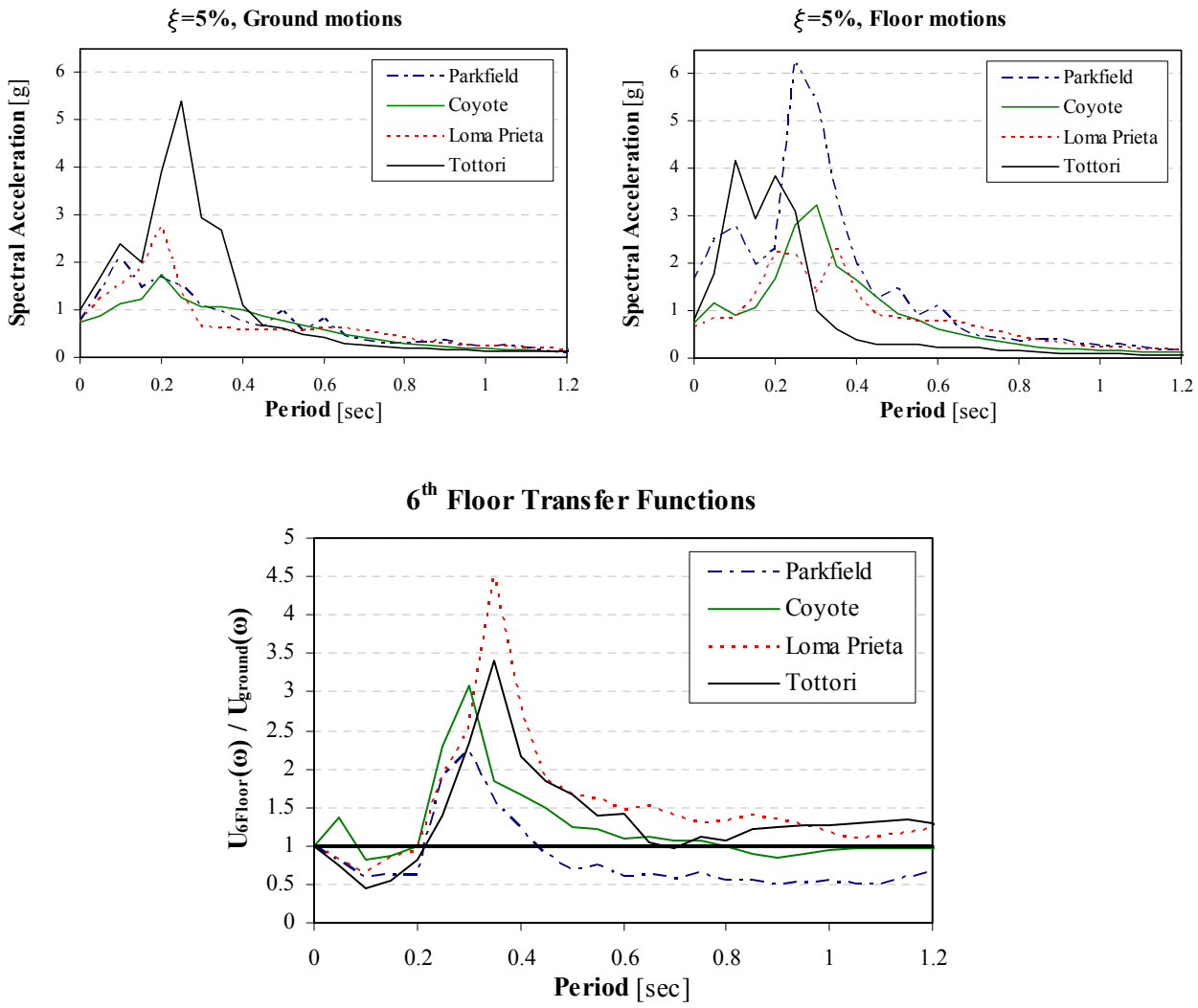

Figure 2-2: Top: Elastic response spectra of the ground motions (left) and 6th floor motions (right). Bottom: Transfer function of the motion between the 6th floor and the ground

3 Description of the tests

This work is based on the experimental tests performed on the shake table at the Earthquake Simulator Laboratory of the Earthquake Engineering Richmond Center in order to investigate the dynamic response of massive equipments under various earthquake motions.

The equipments tested (Figure 3-1) are three and their geometric properties are reported in Table 3-1.

Table 3-1: Geometric properties of the equipment

Equipment	**Type**	$2h$ [cm]	$2b$ **x** $2l$ [cm]
ASP	refrigerator	180.3	76.2 x 58.4
FORMA	incubator	228.6	92.7 x 62.2
KELV	refrigerator	213.4	63.5 x 66.0

The tests were performed using not only the recorded ground and floor motions (listed in Table 2-1) but also pulse excitations. The interest in the response to a pulse tests is justified by several studies (Campillo et al. 1989, Iwan and Chen 1994, Makris and Rossos 2000) where the possibility to represent the seismic input of near-source motions with the principle coherent long-duration pulses is pointed out.

Figure 3-1: Photographs of the equipments tested on the shake table

4 Idealised model of sliding problem

The sliding of unrestrained rigid block is characterised by a strong non-linearity as shown in the Figure 4-1. This behaviour points out that the most practicable way to analyse the problem consist in a regression of experimental tests in order to define an empirical law between demand (maximum displacement) and an intensity measure.

Simulation tests are affected by the difficult assessment of the friction coefficients (static and dynamic) and furthermore they are based on the assumption of "purely sliding" response (there is no rocking and jumping during excitation period [1]) not confirmed by the experimental tests (Figure 4-2).

The process is non-Gaussian and non stationary and so a stochatistic approach is not applicable.

Rigid Body. The force-displacement relationship of the equipment can be approximated by the model shown in Figure 4-4, where U_Y is the yielding displacement (that can be also equal to zero, in a case of perfect rigid body), Q_y is the yielding force equal to $\mu_s \cdot m \cdot g$ at the beginning and then to $\mu_k \cdot m \cdot g$, where μ_s is the static and μ_k is the kinetic friction coefficient and m is the mass of the body .

In the following we have considered the static friction coefficient as the significant parameter of the mechanical properties of the equipment.

Table 4-1: Mechanical properties of the equipments

Equipment	μ_s	μ_k	u_Y [cm]	$Weight$ [kg]
ASP	0.43	0.31	0.05	??
FORMA	0.3	0.23	0.38	??
KELV	0.37	0.28	0.025	??

Seismic Input. ……
…….
…….
…….

Failure Mode. Unrestrained blocks lose their functionality (fail) when the relative displacement exceeds a certain threshold. The limit state can be expressed by:

$$\left|D_{Max}\right| \geq c\,, \tag{4-1}$$

where c is the displacement threshold. In the following we have considered three set equals to $c = 7.5\ cm$, $c = 15\ cm$ and $c = 22.5\ cm$ (around 3, 6 and 9 *inches*).

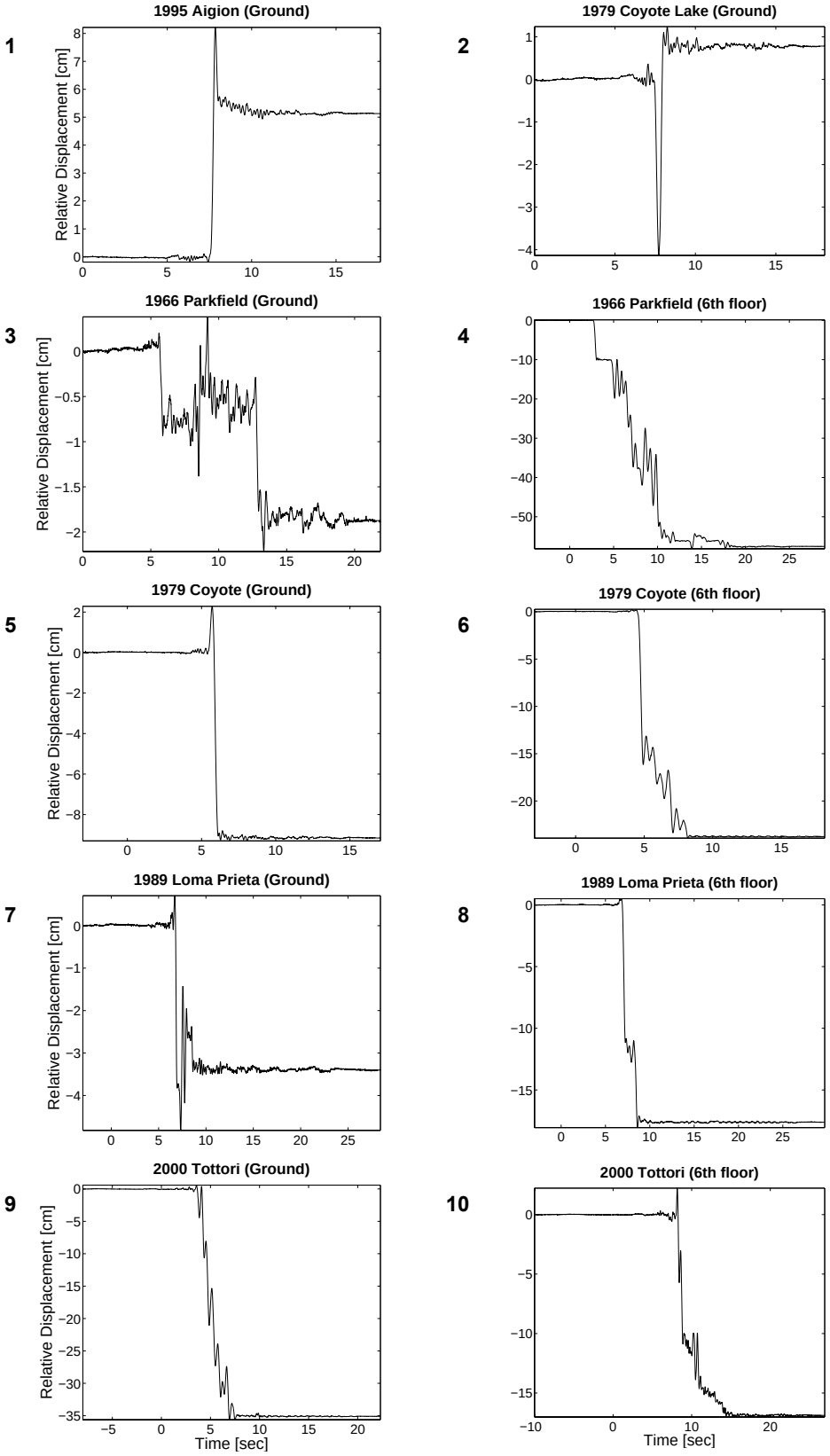

Figure 4-1: Relative Displacement response histories of the free-standing ASP equipment when subjected to the motions used in this study

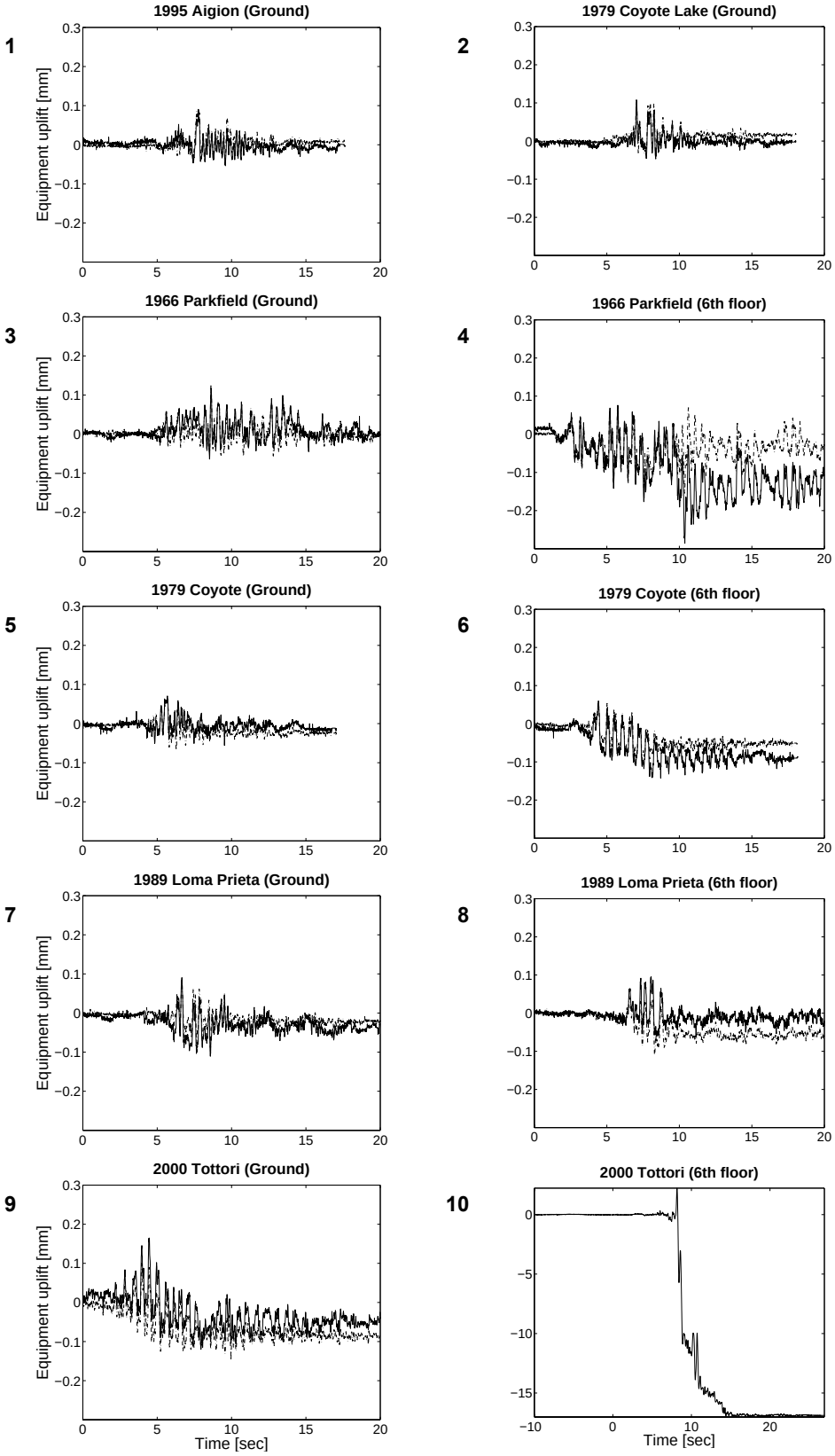

Figure 4-2: Uplift response histories of the free-standing ASP equipment when subjected to the motions used in this study

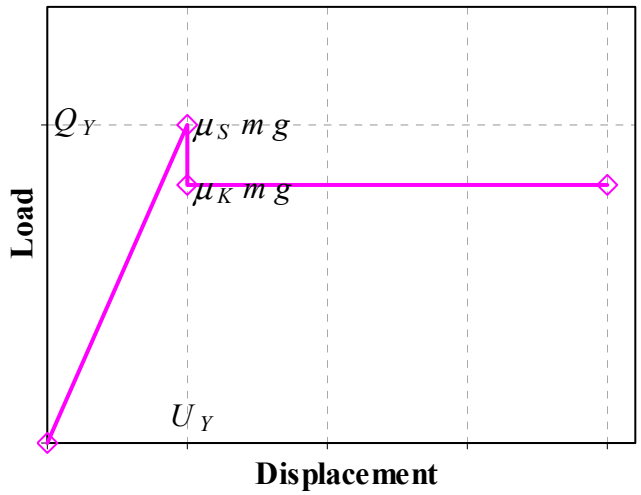

Figure 4-3: ……..

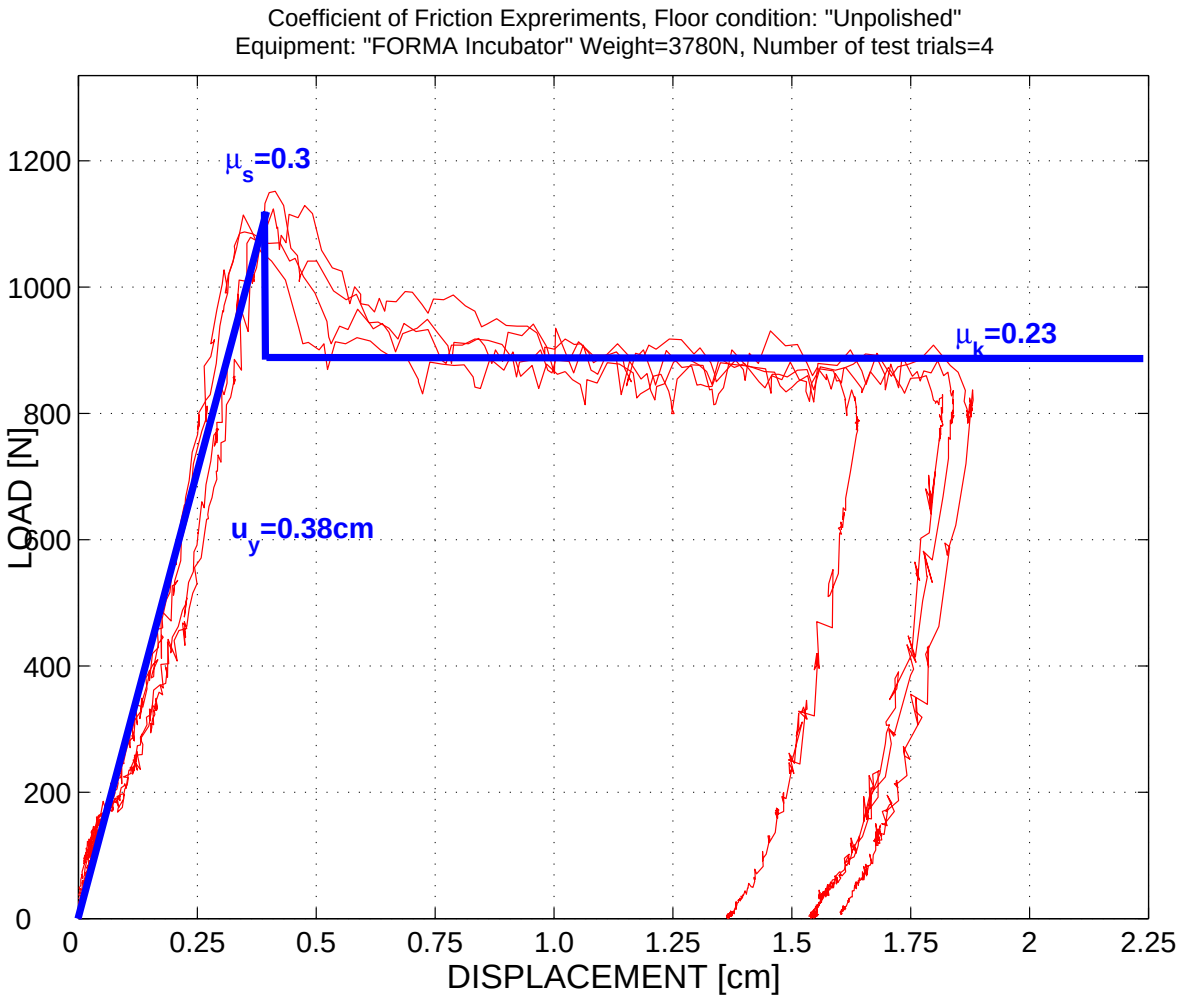

Figure 4-4: Force-Displacement Relationship

5 Experimental Fragility Curve in function of PGA

5.1 Regression on experimental results

We have assumed that the median value of the demand, $\hat{D}$, can be approximately expressed as a function of a chosen intensity measure, IM, by

$$\hat{D} = a_0 + a_1 \cdot IM \,, \tag{5-1}$$

where a_0 and a_1 was determined by a regression at least square on the experimental data.

The demand D is assumed to be log-normally distributed about the median, with standard deviation of the natural logarithms ("dispersion") equal to σ and consequent $\sigma_{ln} = \sqrt{ln\left(1 + \left(\frac{\sigma}{\hat{D}}\right)^2\right)}$.

The random variable D can so expressed by

$$D = \left(a_0 + a_1 \cdot IM\right) \cdot \varepsilon \,, \tag{5-2}$$

where ε is a log-normal random variable with unit median and dispersion equal to σ_{ln}.

We have performed the regression on the experimental result for all the equipments and in order to take in account the different characteristics we have defined the intensity measure as

$$IM = PTA / g - \mu_s \tag{5-3}$$

and the Demand as

$$D = \max\left(Disp\right) - u_y \,. \tag{5-4}$$

On the basis of the (5-2) and (5-3) the (5-1) can be simplified in

$$D = \left(a_1 \cdot IM\right) \cdot \varepsilon \,, \tag{5-5}$$

where $a_0 = 0$.

From the regression, reported in , we found $a_1 = 32.23$ and $\sigma = 8.65\ cm$.

It's worth to point out that:

a) although the value of standard deviation is quite high, it's due to the large variability of frequency content of ground motions with same PGA;
b) the validity of this relation is limited in the range of the friction coefficient ($0.25 \le \mu \le 0.5$).

The Kolmorogov-Smirnoff test [7] was preformed to validate the log-normal distribution adopted in this study. In order to not reject the adopted distribution the maximum difference between the empirical cumulative distribution function (CDF), $F_n(i)$, and the CDF of the adopted distribution, $F(i)$, should be not greater than the reference value $R_k(\alpha)$,

$$R = max(F_n(i) - F(i) | F_n(i-1) - F(i)) \le R_k(\alpha), \quad (7)$$

where k is the number of experiments and α is the level of significance.

In the examined case k is equal to 27 and so the references values for different levels of significance are $R_{27}(0.2,0.1,0.01) = (0.20,0.23,0.305)$. The maximum difference R is equal to 0.1289; so the log-normal distribution can be adopted to describe the random variable Demand.

5.2 Derivation of fragility curve

The fragility function is defined as the probability of failure, P_f, conditional on one parameter defining the intensity of the intensity of the motion. The P_f corresponds to the probability of exceeding of the demand, D, a certain threshold (capacity), C, for a given intensity and friction coefficient; on the assumption that the demand is log-normally distributed, it's given by:

$$P_f = 1 - P(D \le C) = 1 - \Phi\left(\frac{ln\, C - \lambda}{\varsigma}\right), \quad (7)$$

where λ, ς are the parameter of the distribution function of $\hat{D} = a_1 \cdot IM$ and σ_{ln}.

The capacity is represented by a certain displacement threshold (deterministic).

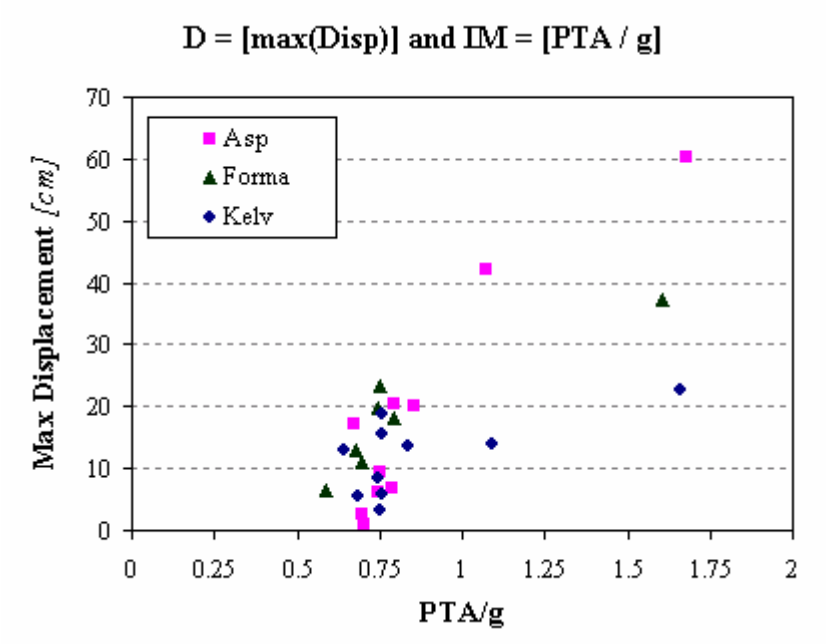

Figure 5-1: Results for D = Max(D) and IM = PTA/g

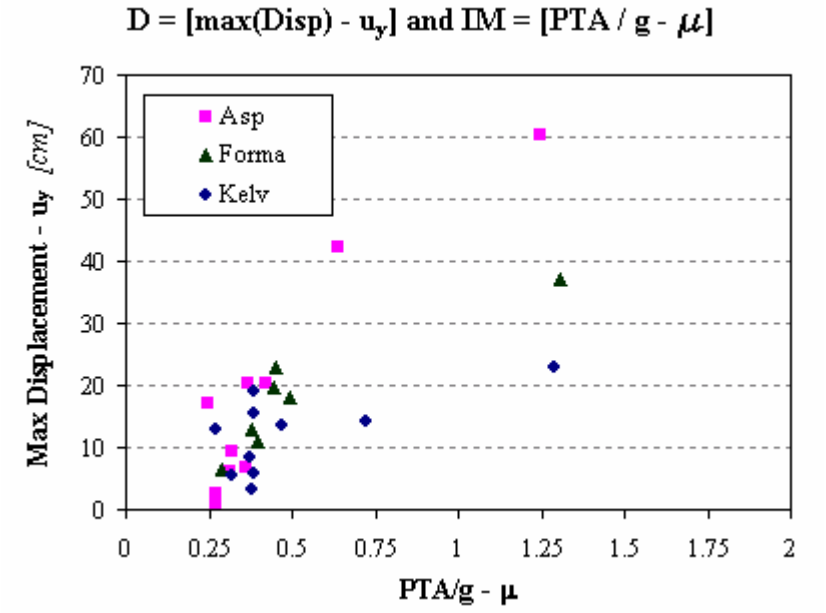

Figure 5-2: Results for D = Max(D) – U_Y and IM = PTA/g -μ_s

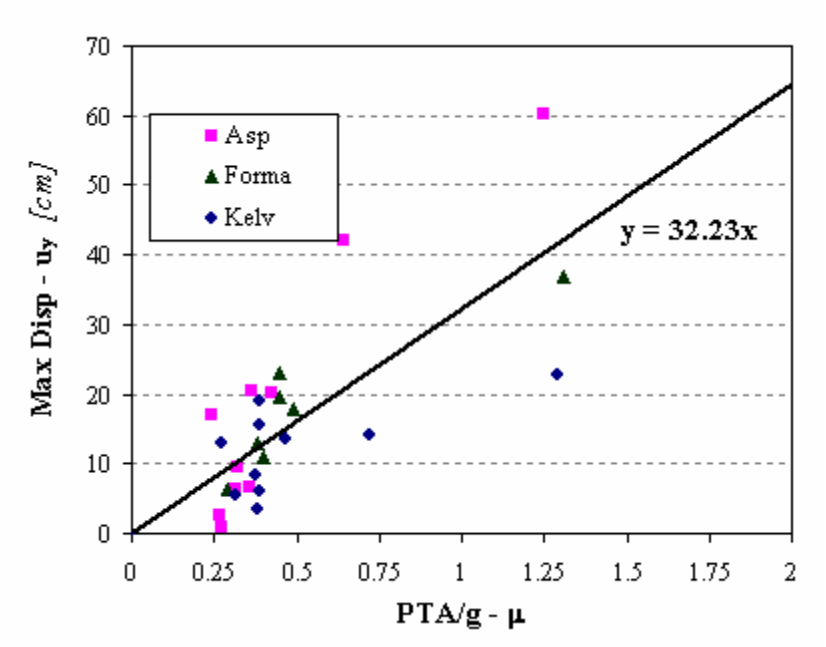

Figure 5-3: Regression on experimental data

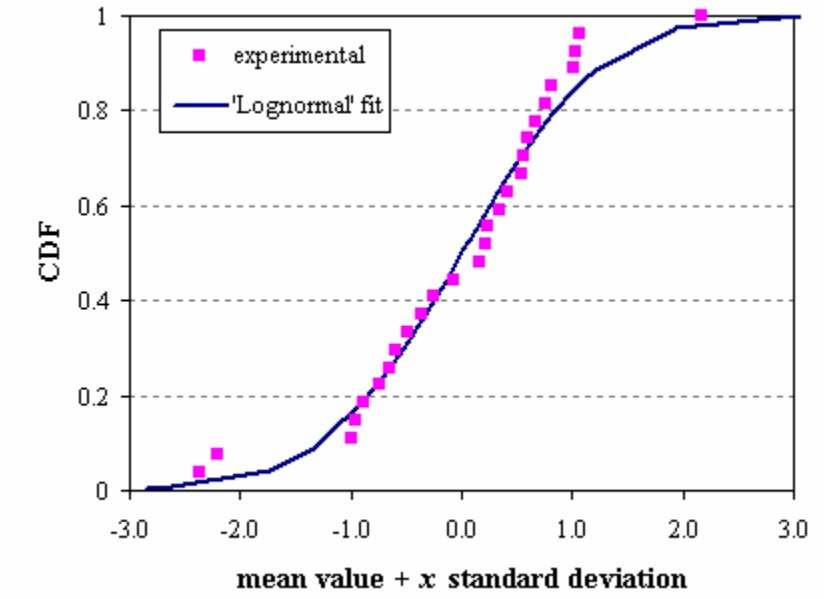

Figure 5-4: Comparison of experimental and fitted CDF

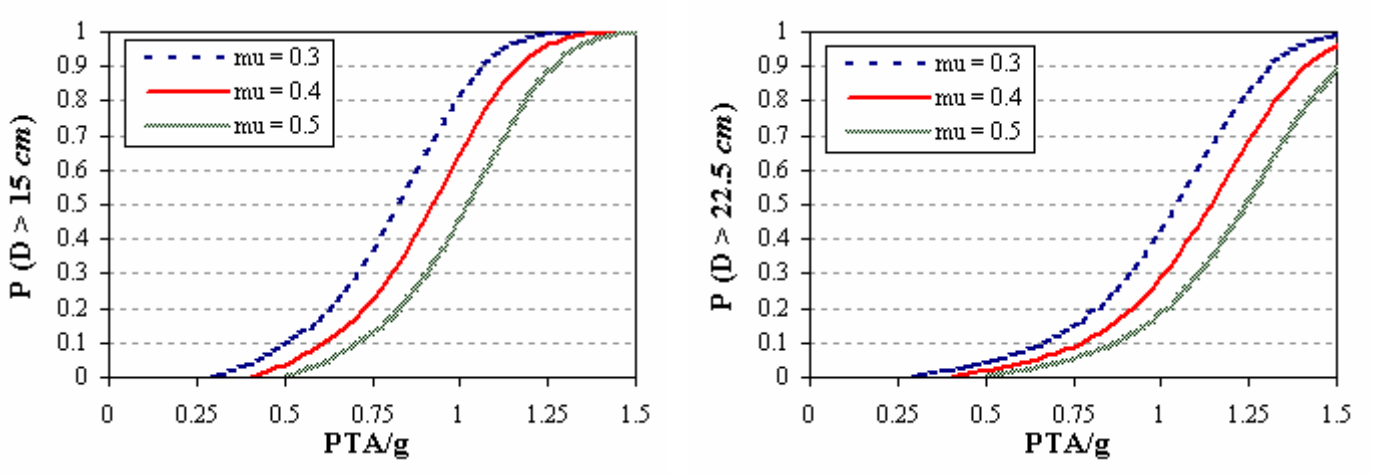

Figure 5-5: Fragility curves for threshold equal to 15 *cm* at left and 25.5 *cm* at right

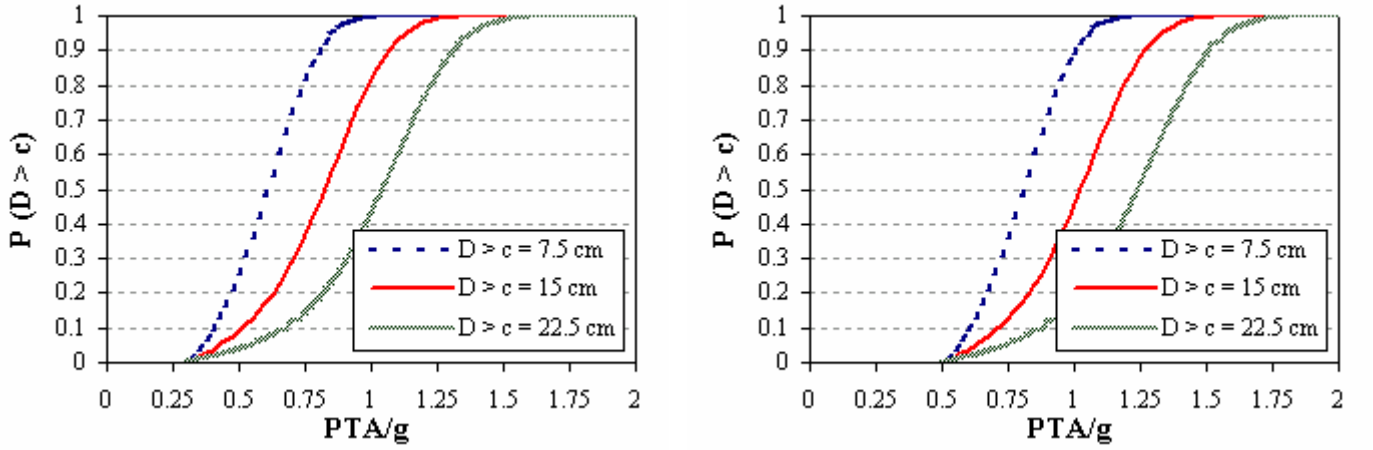

Figure 5-6: Fragility curves at different value of static friction coefficient (0.3 at left, 0.5 at right)

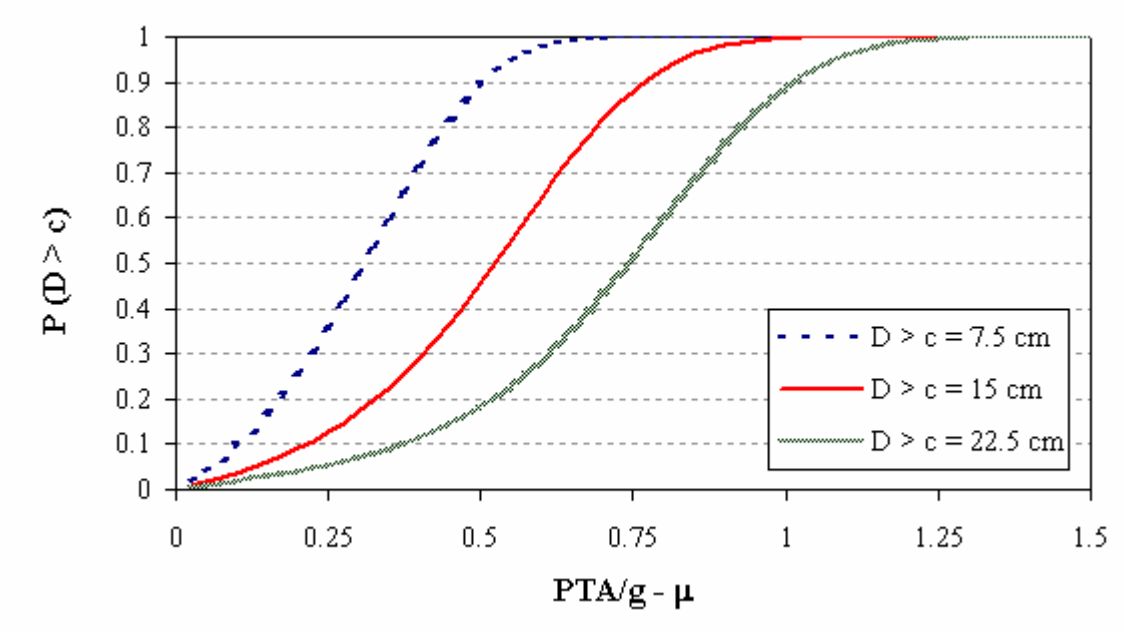

Figure 5-7: Fragility curves for different thresholds

6 Additional study for source ground motions

The peak acceleration is an useful measure of the intensity of an earthquake motion but it doesn't resume all the characteristics that have influence in the sliding problem, as it is confirmed from the high values of the standard deviation of the regression presented in section 5.1.

In the case of sliding the frequency content has great importance. In Figure 6-2 we have reported the results for the pulse-tests and the dependence of the maximum displacement from the frequency is clearly pointed out. As expected at the same peak base acceleration excitations with higher frequency produce smaller sliding-displacement.

In the following an alternative descriptions of the seismic motion based on the approximation with trigonometric pulses is investigated.

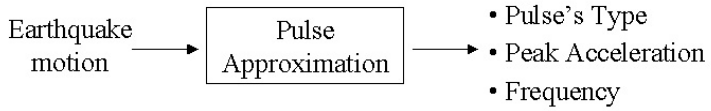

Figure 6-1: Scheme of the pulse-approximation

The validity of this representation is limited to near-field motions, in which the kinematic characteristics often contain large displacement pulses and in some case the coherent pulse is not only distinguishable in displacement and velocity histories but also in acceleration history.

In Figure 6-2 the acceleration, velocity and displacement shapes for different type of pulses (forward pulse, type A; forward-and-back pulse, type B; type C1; type C2) are shown.

A thorough analytical description is given in [6]. Here it's worth to report only that the displacement of a forward-and-back pulse has the same shape as the velocity of a forward pulse and similarly the displacement of a type C1 pulse resembles the shape of the velocity of a forward-and-back pulse and the shape of acceleration of a forward pulse. This shows that type C pulses provide a continuous transition from cycloidal pulses to harmonic steady-state motions [6].

The validity of this approach is confirmed by the experiment results, where it's come out the fundamental role played by the first pulse, responsible for most part of the displacement.

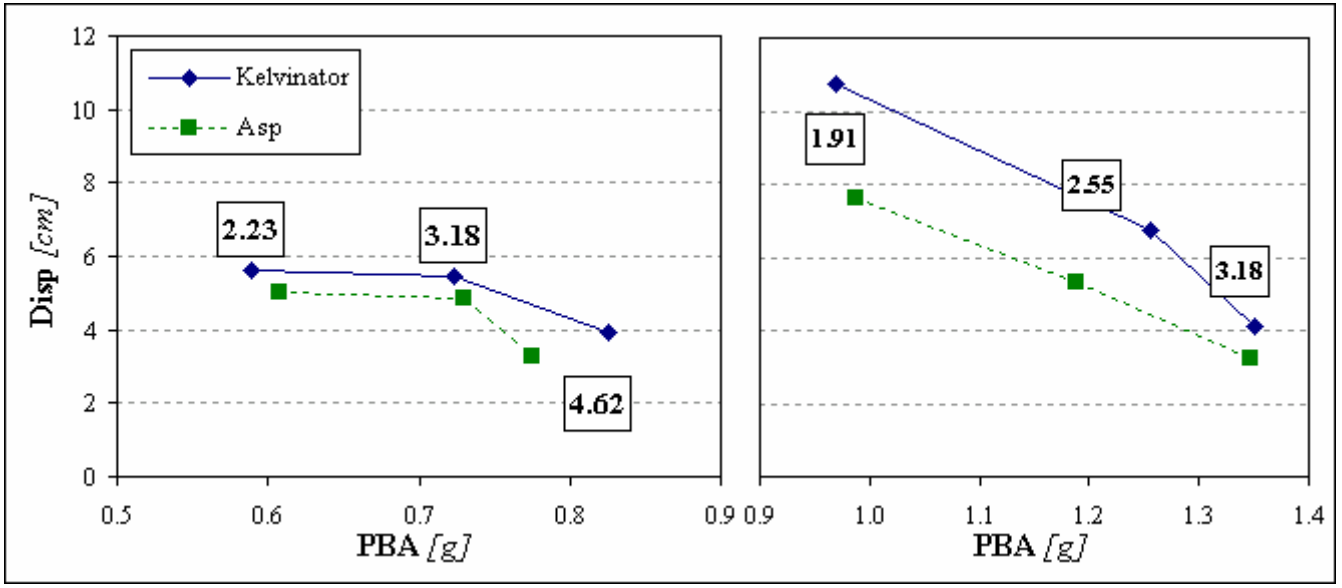

Figure 6-2: Importance of the frequency content in the seismic sliding response (at left Type A pulses, at right Type B pulses)

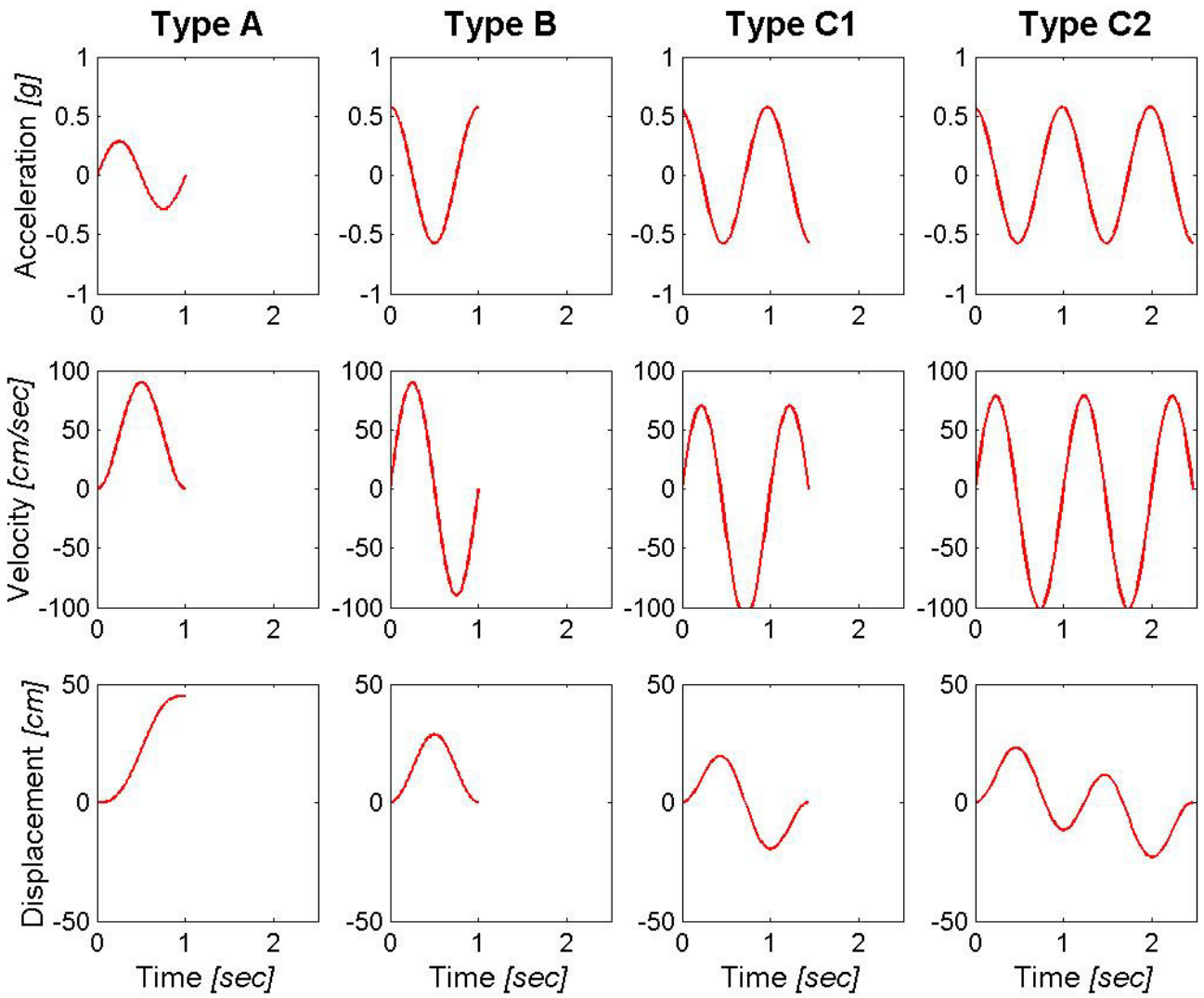

Figure 6-3: Acceleration, velocity and displacement time histories of cycloidal pulses Type A (first column), Type B (second col.), Type C_1 (third col.) and Type C_2 (fourth col.) for same velocity and frequency

In
Figure 4-1 we have reported the time histories of the relative displacement for one of the three equipments (ASP). For the others two the results are roughly the same.
In the records 1, 2, 5 and 7 (all ground motions) all the sliding displacement is due to only one pulse and so they can be approximated by Type A or Type B pulses; for the records 6, 8, 9 and 10 the maximum relative displacement is a sum of the contribute of a sequence of pulses (harmonic excitation) and this behaviour can be represented by Type C pulses; the records 3 and 4 don't show a coherent pulse in acceleration and in velocity either and so we have neglected them.
The "approximation" parameters, (1) Type of the pulse, (2) Peak of Acceleration and (3) Frequency, of the ground motions considered in this study are listed in Table 6-1.

This description points out the differences between the ground and floor excitations (Figure 2-1). On one side the ground motions usually are characterised by a fundamental pulse and so they have been approximated by Type A or Type B pulses; on other side the floor motions exhibit an harmonic trend and consequently they are well described by pulses of Type C (Table 6-1).
The structure acts as a filter modifying the frequency content and the PA. Generally the frequency of a floor motion tends to be concentrated around the fundamental period of the structure, T_f, and the PA can be related to the PGA by an amplification factor.

In first instance a rough approximation of the floor motion can be done assuming a Type C pulse with PA equal to PGA and the inverse of the fundamental period as frequency, $f = 1/T_f$ (Figure 6-4 a). More accurate results (Figure 6-4 b) can be obtained by performing a limited number of nonlinear dynamic analyses of the building, from which it's possible:

- to assess the mean value of the amplification factor;
- to relate the fundamental frequency in function of the intensity of the seismic motion.

In the examined cases, for LSA building and the sixth floor, it's equal to $AF_6 = 1$.

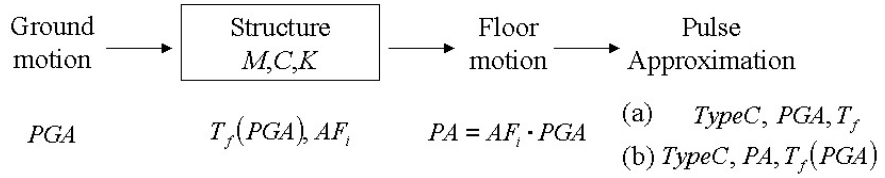

Figure 6-4: Pulse-approximation for a floor motion

Table 6-1: Approximation of earthquake with trigonometric pulses

Kelv	**PBA** *[g]*	**Disp** *[cm]*	**Type**	**Amplit.** *[g]*	**Vel** *[cm/sec]*	**Freq** *[Hertz]*	**T** *[sec]*
Aegion	0.755	15.43	B	0.760	-71.1	1.7	0.59
Coyote Lake	0.686	5.52	A	0.511	-81.3	2.0	0.50
Parkfield (ground)	0.794	3.40	-	-	-	-	-
Parkfield (6th floor)	1.662	22.83	-	-	-	-	-
Coyote (ground)	0.744	8.41	A	0.558	88.9	2.0	0.50
Coyote (6th floor)	0.756	18.94	C1	0.613	61.0	1.6	0.63
Loma Prieta (ground)	0.756	5.95	A	0.511	81.3	2.0	0.50
Loma Prieta (6th floor)	0.642	13.03	C1	0.586994	-58.4	1.6	0.63
Tottori (ground)	1.092	14.08	C2	0.755	-55.9	2.2	0.47
Tottori (6th floor)	0.839	13.60	C2	0.734	-50.8	2.3	0.43
Forma	**PBA** *[g]*	**Disp** *[cm]*	**Type**	**Amplit.** *[g]*	**Vel** *[cm/sec]*	**Freq** *[Hertz]*	**T** *[sec]*
Aegion	0.793	18.04	B	0.705	-66.0	1.7	0.59
Coyote Lake	0.681	13.11	A	0.511	-81.3	2.0	0.50
Parkfield (ground)	0.698	11.10	-	-	-	-	-
Parkfield (6th floor)	1.609	37.19	-	-	-	-	-
Coyote (ground)	0.747	19.83	A	0.558	88.9	2.0	0.50
Coyote (6th floor)	0.750	23.25	C1	0.613	61.0	1.6	0.63
Loma Prieta (ground)	0.731	11.46	A	0.479	76.2	2.0	0.50
Loma Prieta (6th floor)	-	-	-	-	-	-	-
Tottori (ground)	-	-	-	-	-	-	-
Tottori (6th floor)	-	-	-	-	-	-	-
Asp	**PBA** *[g]*	**Disp** *[cm]*	**Type**	**Amplit.** *[g]*	**Vel** *[cm/sec]*	**Freq** *[Hertz]*	**T** *[sec]*
Aegion	0.745	8.22	B	0.705	-66.0	1.7	0.59
Coyote Lake	0.700	4.14	A	0.527	-83.8	2.0	0.50
Parkfield (ground)	0.702	2.22	-	-	-	-	-
Parkfield (6th floor)	1.677	58.13	-	-	-	-	-
Coyote (ground)	0.749	9.30	A	0.574	91.4	2.0	0.50
Coyote (6th floor)	0.796	23.93	C1	0.638	63.5	1.6	0.63
Loma Prieta (ground)	0.768	4.82	A	0.527	83.8	2.0	0.50
Loma Prieta (6th floor)	0.675	18.05	C1	0.587	-58.4	1.6	0.63
Tottori (ground)	1.071	35.63	C2	0.789	-58.4	2.2	0.47
Tottori (6th floor)	0.853	17.02	C2	0.807	-55.9	2.3	0.43

7 Experimental Fragility Curve in function of PULSE

7.1 Regression on experimental results

Analogously to the regression presented in section 5.1 we have adopted the simplified relation (5-4), defining the intensity measure by:

$$IM = \left(PA/g - \mu_s\right)/f^2 , \tag{7-1}$$

where PA, the peak of the acceleration of the time history, and f, the frequency, are parameters of the pulse-approximation; and the Demand by:

$$D = \max\left(Disp\right) - u_y . \tag{7-2}$$

The meaning of (7-1) can be figured out by the two limit cases $f = 0$ and $f = \infty$.

For $f \to 0$ the excitation becomes static and so when the load exceeds the yielding force, $Q_Y = \mu_S mg$, the relative displacement tend to be infinity and consequently the probability of exceeding any threshold is 1; on other side when $f \to \infty$ the probability is always 0 for any intensity of the load.

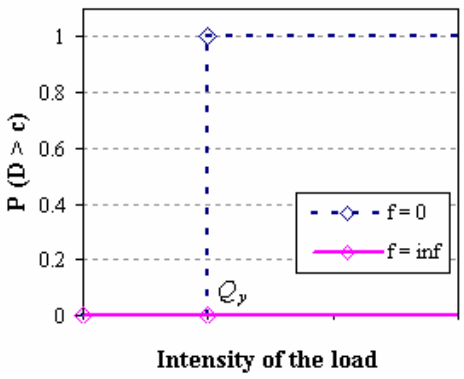

Figure 7-1: Fragility curve for the limit cases ***f = 0*** and ***f = ∝***

At first a validation of (7-1) and (7-2) on the basis of results of the pulse-tests is reported and then the regression on all the results, including the trigonometric approximation resumed in Table 6-1, is performed.

Figure 7-2 shows the different representation of the results; at left in function of PGA and at right in function of the selected intensity measure. The dispersion of the trend line for both Type A and Type B pulses is very low: $\sigma_{TypeA} = 0.72\ cm$ and $\sigma_{TypeB} = 1.31\ cm$.

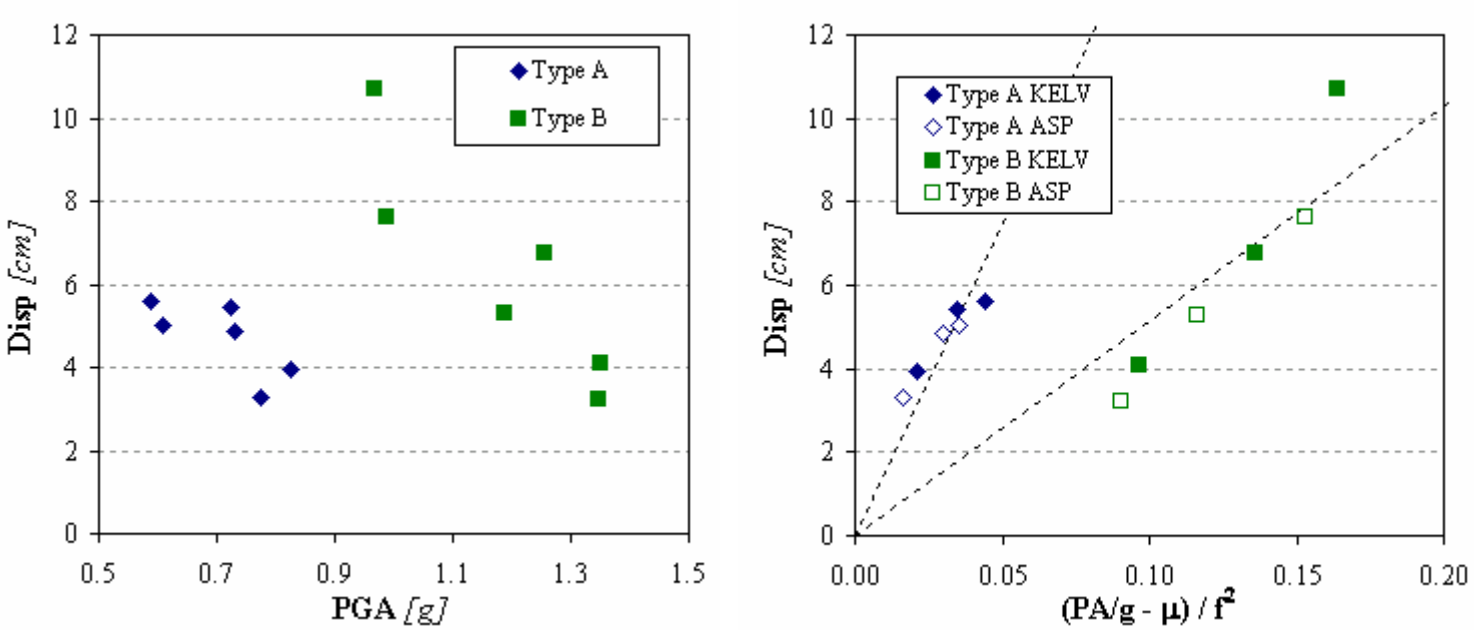

Figure 7-2: Results of pulse-tests in function of the *PGA* (at left) and of *IM* (at right)

For the “approximated” pulses a clarification of the definition of the peak acceleration, PA, is necessary. In fact it’s possible to use either the peak acceleration that comes out from the “right” pulse approximation, Amp (Figure 7-3 at left), or the maximum acceleration of the time histories, peak base acceleration, PBA (Figure 7-3 at right).

Figure 7-4 shows the consequence of the two different choices: in the first case, $PA = Amp$, we underestimate the sliding displacement and so the points are placed at left of the trend line of the “true” pulses; in the second the behaviour is the opposite.

The reason of that is explained in Figure 7-3 where it’s possible to see how in the first approximation we loose some part of the time history while in the second we add something that doesn’t exist.

In order to agree with the literature where the hazard function are expressed in function of the peak of the time histories we have adopted the PBA as PA. It’s important to note that for the ground motion the terms PBA corresponds to PGA, while for the floor motions it can be related to PGA by $PBA = AF_i \cdot PGA$, where AF_i is the amplification factor for the floor level i.

From Figure 7-5 where all the result are synthetically reported it is worth to note that:

- the maximum response for the ground motion (approximated with Type A or Type B) is due to the Type A earthquakes;
- the “harmonic” excitation, described by Type C pulses, produce the largest displacements.

Starting from the assumption that we can predict the maximum acceleration but not the type of the pulses we‘re going to present two different solutions: one for the ground motions and the second one for the floor motion.

In the case of ground motions we have operated a regression on the results of “Type A Pulse” and of the “Type A Eq” (Figure 7-6) and for the floor motions we have taken in account the “Type A Pulse” and the “Type C Eq” results (Figure 7-7).

7.2 Derivation of fragility curve

The fragility curve was derived following the same procedure illustrated in section 5.2 for the same three threshold (7.5, 15.0 and 22.5 *cm*). Below we have just reported some graphs to point out the difference when some parameters (frequency, Figure 7-8 and Figure 7-9, or static friction coefficient, Figure 7-10 and Figure 7-11) change.

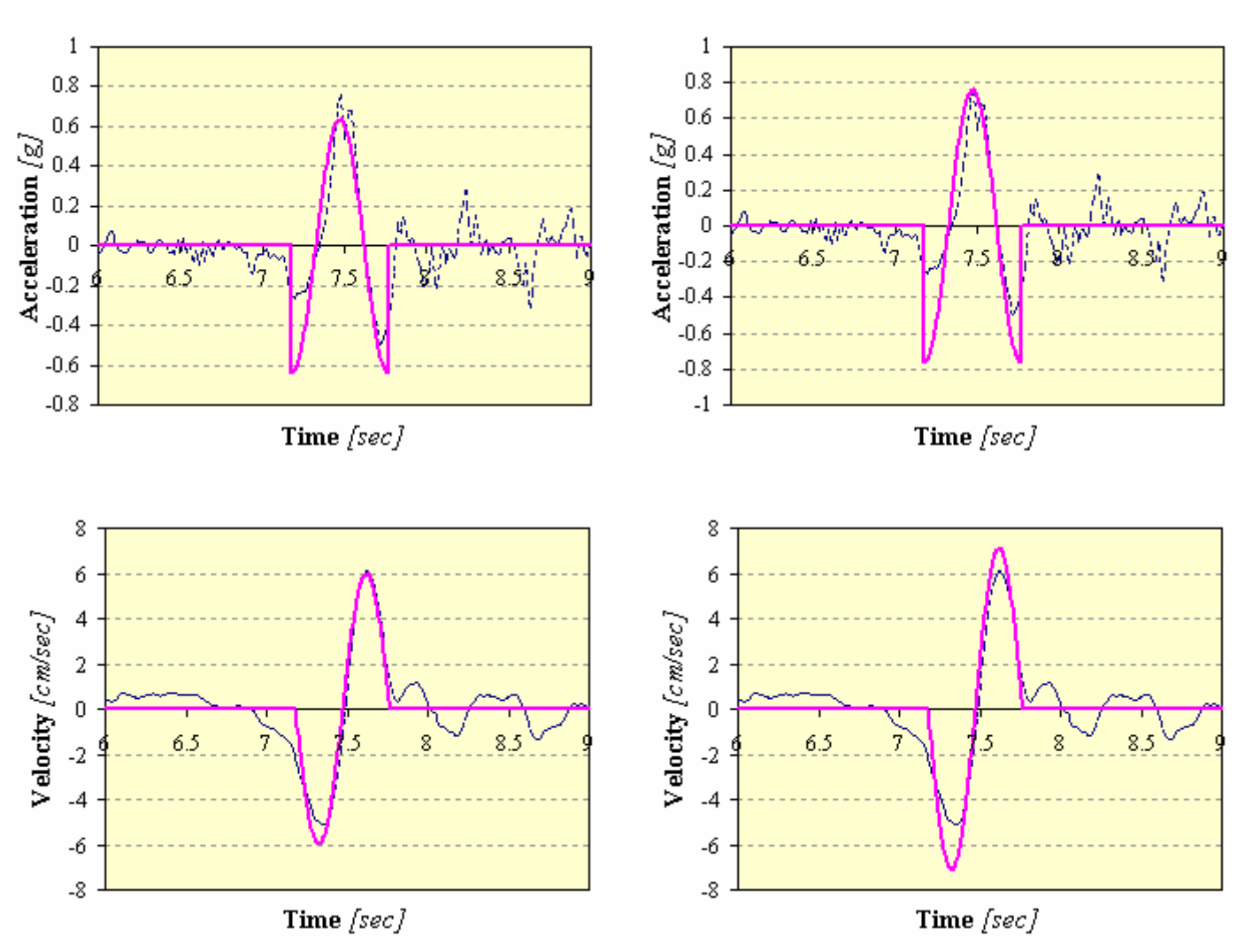

Figure 7-3: Approximation of the earthquake on Velocity (at left) or on Acceleration (at right) for Aegion motion and KELV equipment; Amplitude = 0.636***g*** and PBA = 0.755***g***

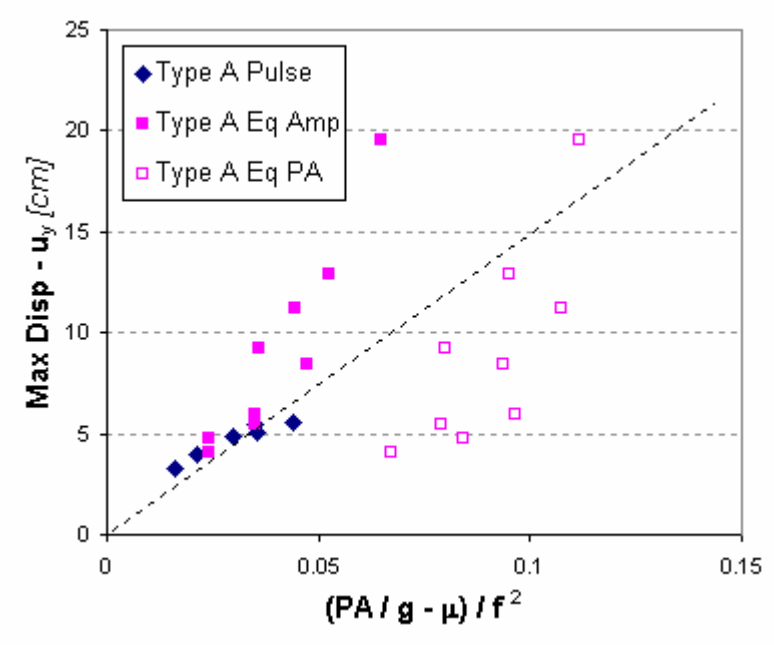

Figure 7-4: Difference in the definition of Peak Acceleration

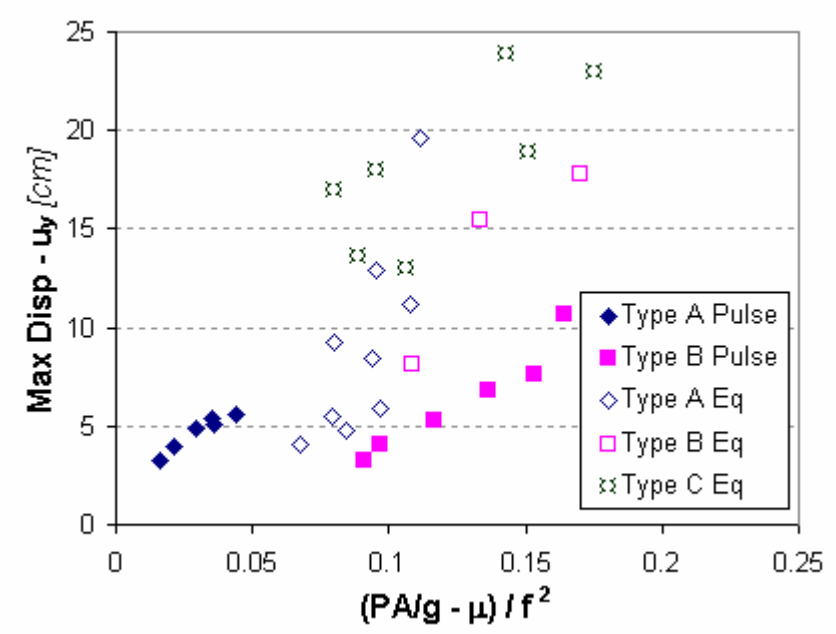

Figure 7-5: Representation of all the experiments for the selected *IM*

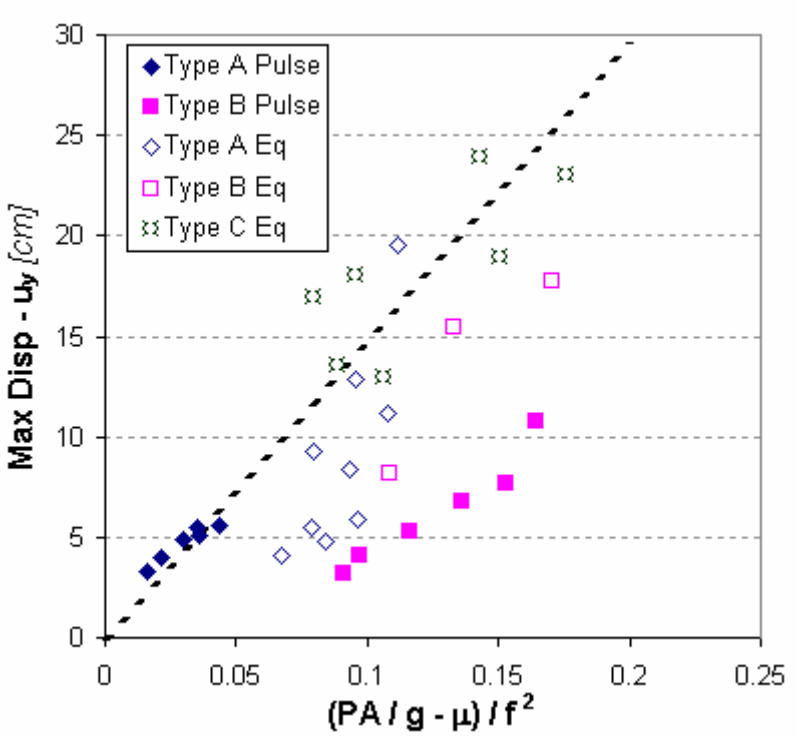

Figure 7-6: Regression for the ground motions: $a_1 = 108.89$ and $\sigma = 3.14\ cm$

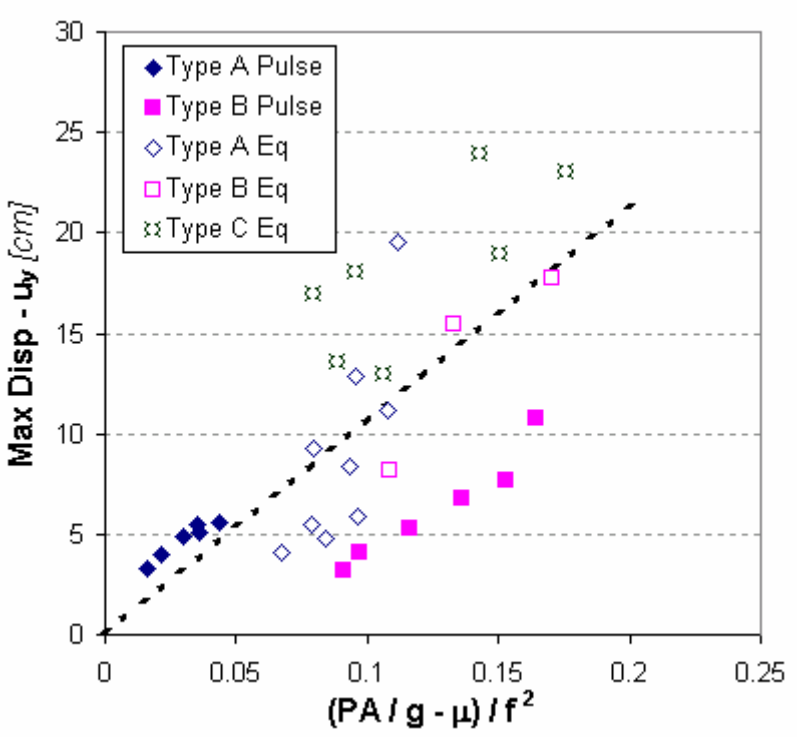

Figure 7-7: Regression for the floor motions: $a_1 = 146.89$ and $\sigma = 4.14\ cm$

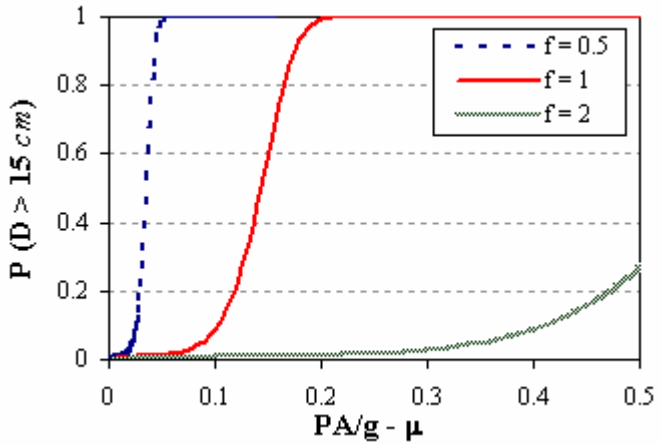

Figure 7-8: Fragility curves for ground motions at different frequency

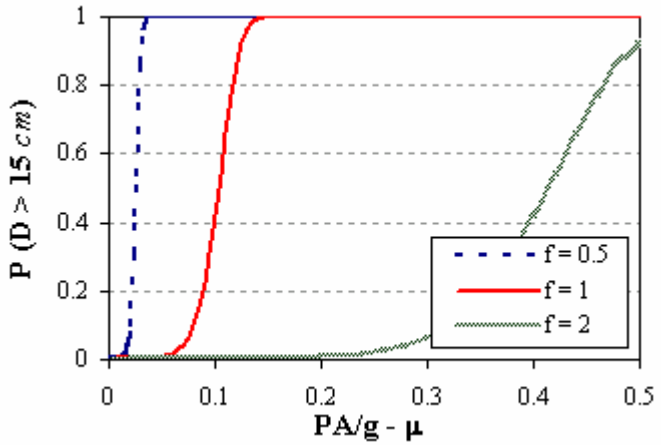

Figure 7-9: Fragility curves for floor motions at different frequency

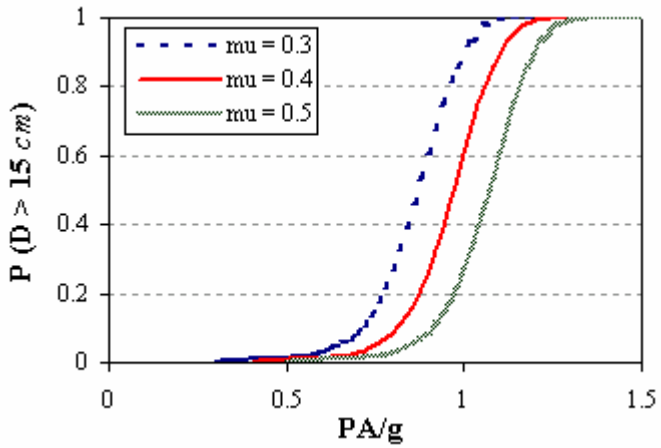

Figure 7-10: Fragility curves for ground motions at different static friction coefficients (f = 2.0 *sec*)

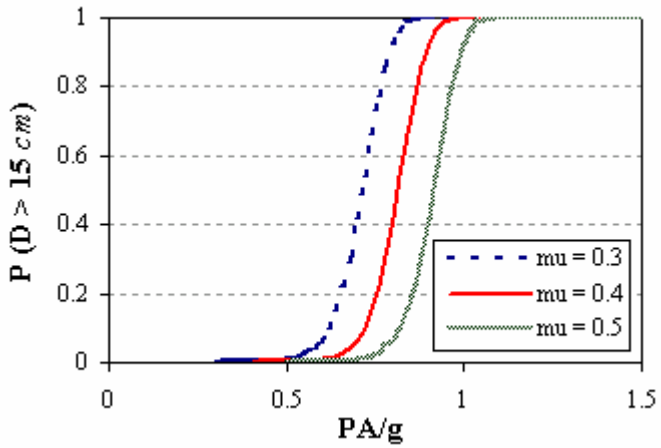

Figure 7-11: Fragility curves for floor motions at different static friction coefficients (f = 2.0 *sec*)

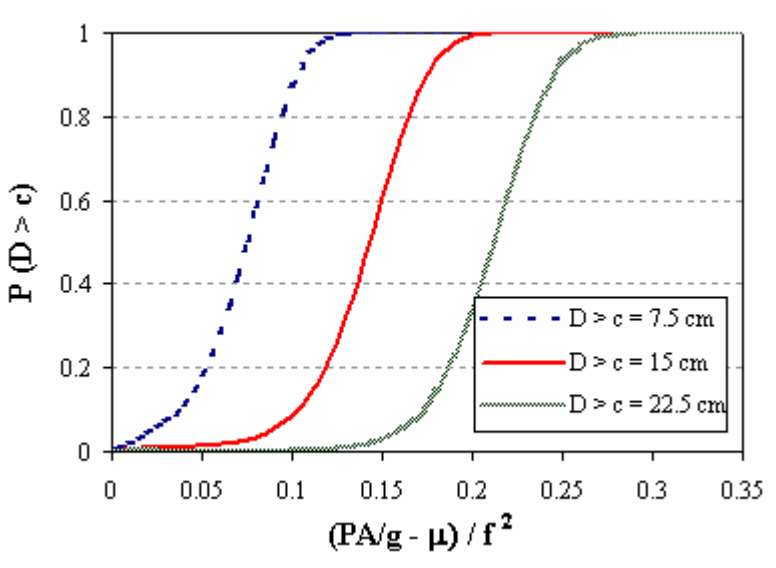

Figure 7-12: Fragility curves for ground motions

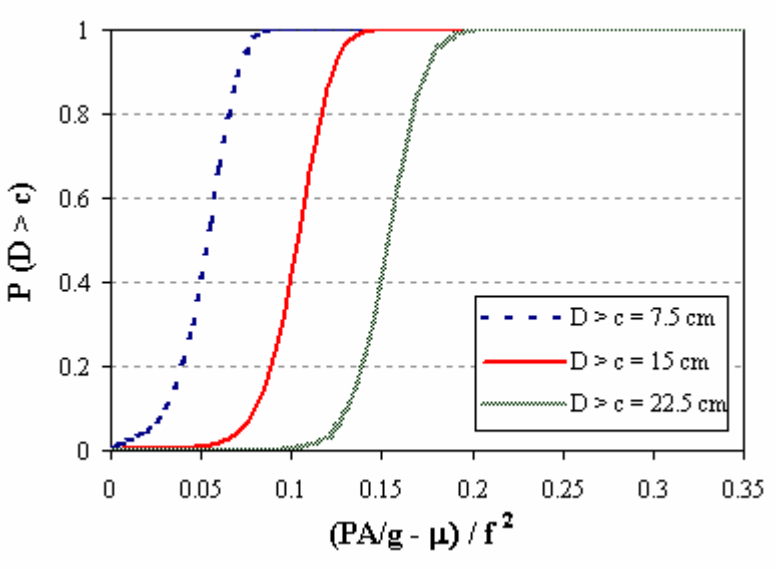

Figure 7-13: Fragility curves for floor motion

8 Conclusions

The principal failure mode of an unrestrained block can be represented by the maximum sliding displacement. The equipment can also rock and so they could also fail for overturning, but the probability of such event is so small that we have neglected it.

The sliding is a phenomenon so complex that analytical simulation has to be based on unrealistic assumption. This study is completely based on results of experimental tests.
The tests were performed using recorded ground motions, ….. floor motions and pulse excitations.

Two solutions are presented:
The first one is general; once the static friction coefficient of the block is assessed, this approach can be easily applied to compute the risk because it's an explicit function of the PGA; the fundamental limit is the high dispersion
The second solution is more complete and has great importance because provide an easy formulation to predict the sliding displacement for the floor motions (where the equipments really are). Nonlinear analysis of building are required to estimate the amplification factor and the variation of the fundamental frequency with the intensity of the excitation. Also this approach provide a fragility curve that defined the properties of the structure and of the block can be expresses as function of only PGA. Consequently the risk can be easily computed by a numerical integration between the fragility curve and the hazard analysis.

All the results presented in this paper are valid for the limited range of friction coefficient that we have investigated ($\mu_S = 0.2 - 0.5$)

9 References

[1] W. H. Chong, and T. T. Soong, 2000 – *Sliding fragility of unrestrained equipment in critical facilities* – Technical Report MCEER-00-0005, Buffalo, NY

[2] P. Bazzurro and C.A. Cornell, 1994 – *Seismic hazard analysis of nonlinear structures: Methodology* – Journal of Struct. Eng, ASCE, 120(11):3320-3344

[3] C. A. Cornell, F. Jalayer, R. O. Hamburger, and D. A. Foutch, 2002 – *The probabilistic basis for the 2000 SAC/FEMA steel moment frame guidelines* – Journal of Struct. Eng., ASCE, 128(4):526-533

[4] D. L. Garcia and T. T. Soong, 2003 – *Sliding fragility of block-type non structural components. Part 1: Unrestrained components* – Earthquake Eng. and Struct. Dyn., 32:111-129

[5] Briefing Paper 5, Seismic Response of Nonstructural Components, Part A – ATC/SEAOC Joint Venture Training Curriculum

[6] N. Makris and Y.S. Rosseau, 2000 – *Rocking response of rigid blocks under near-source ground motions* – Géotechnique 50(3):243-262

[7] D.C. Montgomery and G.C. Runger, 1999 – *Applied Statistics and Probability for Engineers* – John Wiley & Sons

Appendix A Result of pulse approximation

.....
.....
.....
.....

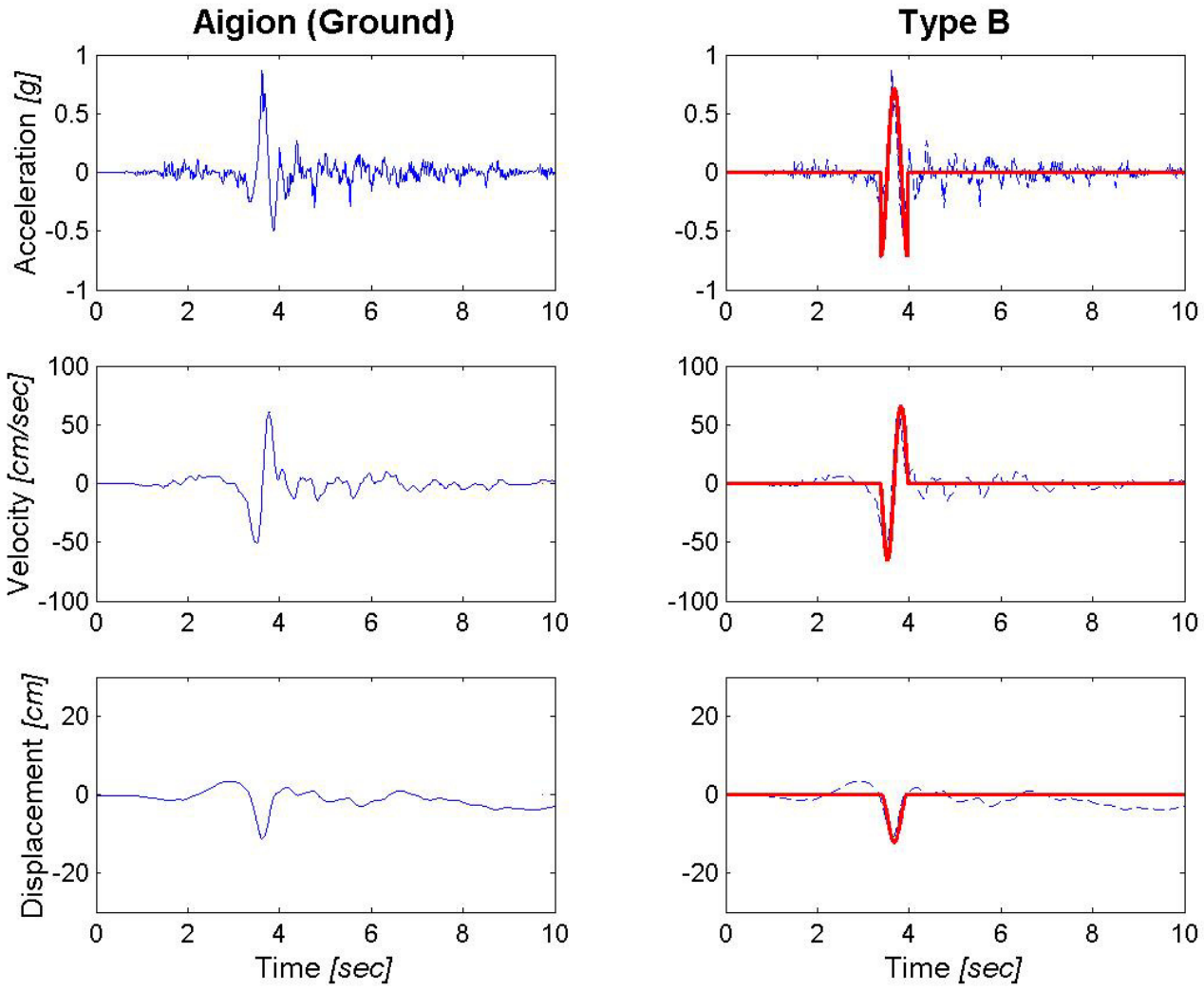

Figure A-1: Acceleration, velocity and displacement time histories recorded of Aigion earthquake (right) and relative pulse approximation (left)

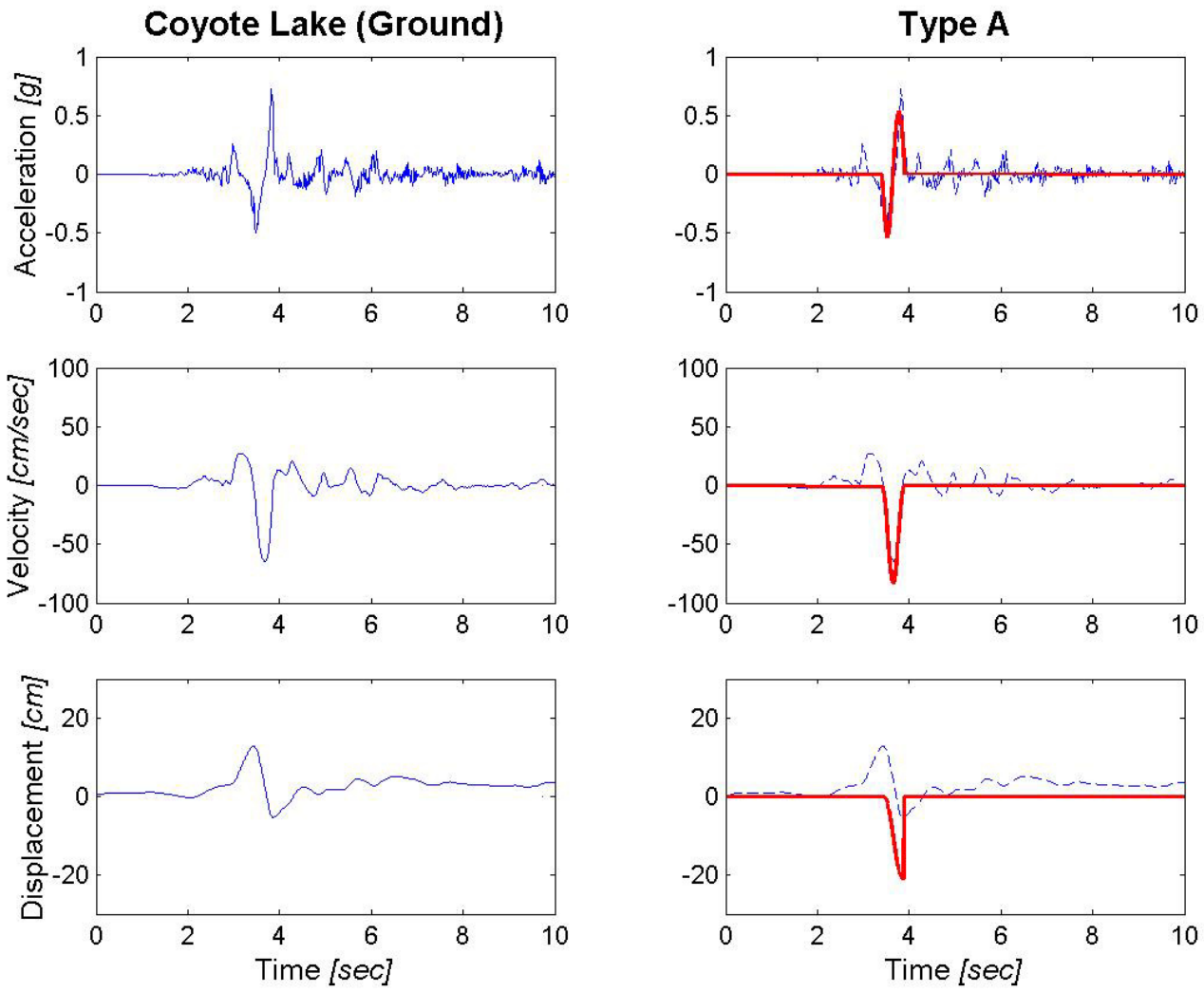

Figure A-2: Acceleration, velocity and displacement time histories recorded of Coyote Lake (ground) earthquake (right) and relative pulse approximation (left)

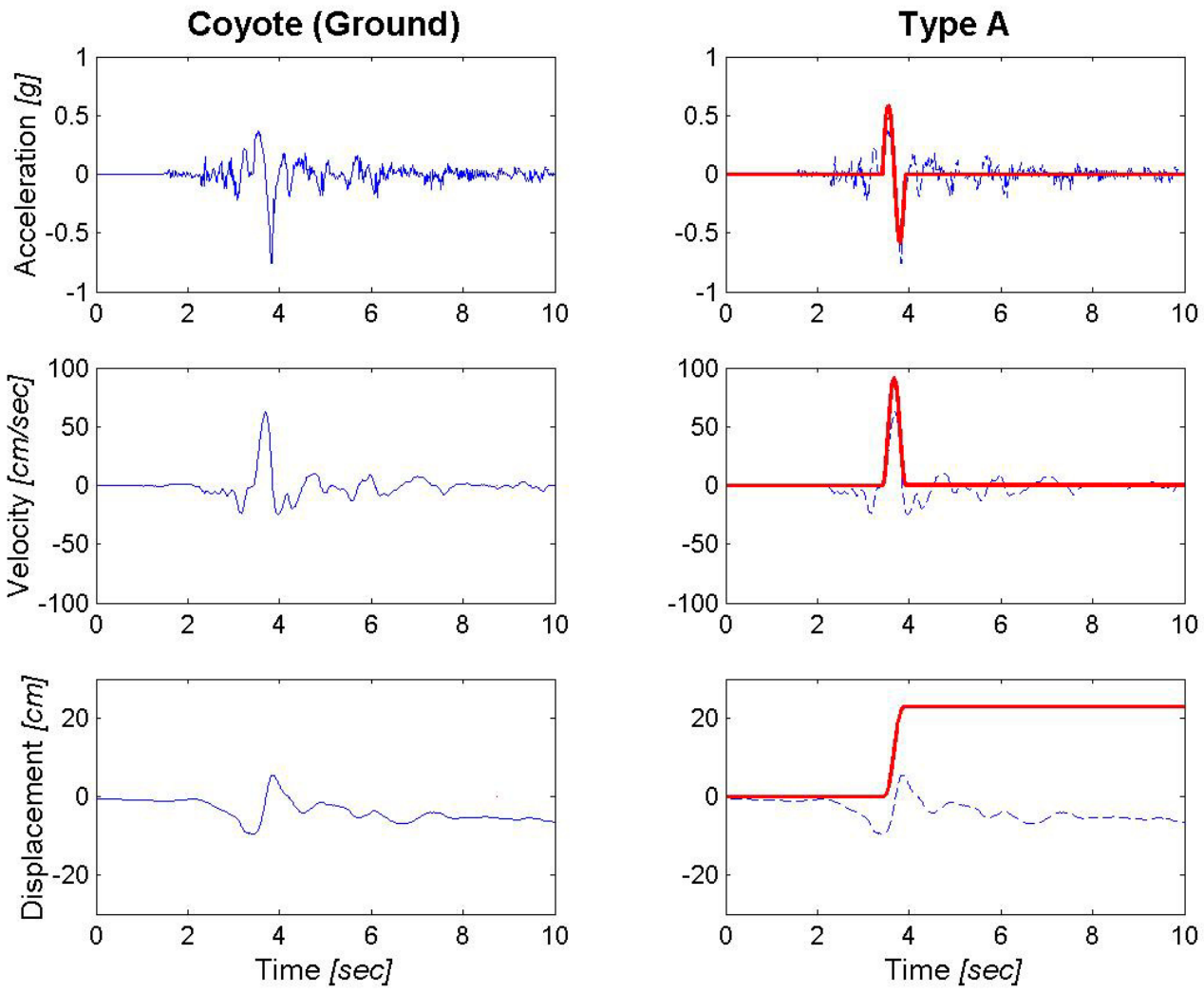

Figure A-3: Acceleration, velocity and displacement time histories recorded of Coyote (ground) earthquake (right) and relative pulse approximation (left)

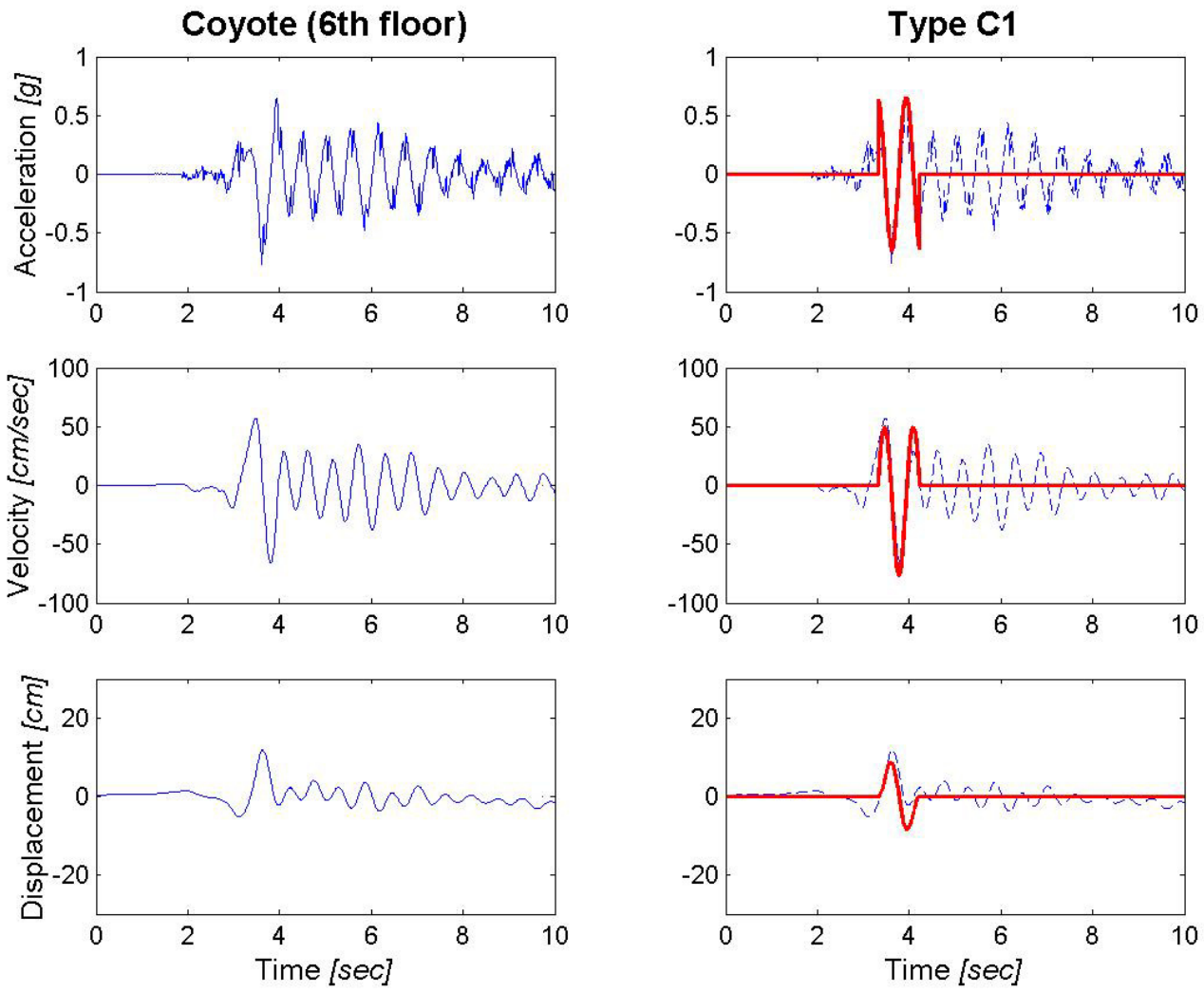

Figure A-4: Acceleration, velocity and displacement time histories recorded of Coyote (6th floor) earthquake (right) and relative pulse approximation (left)

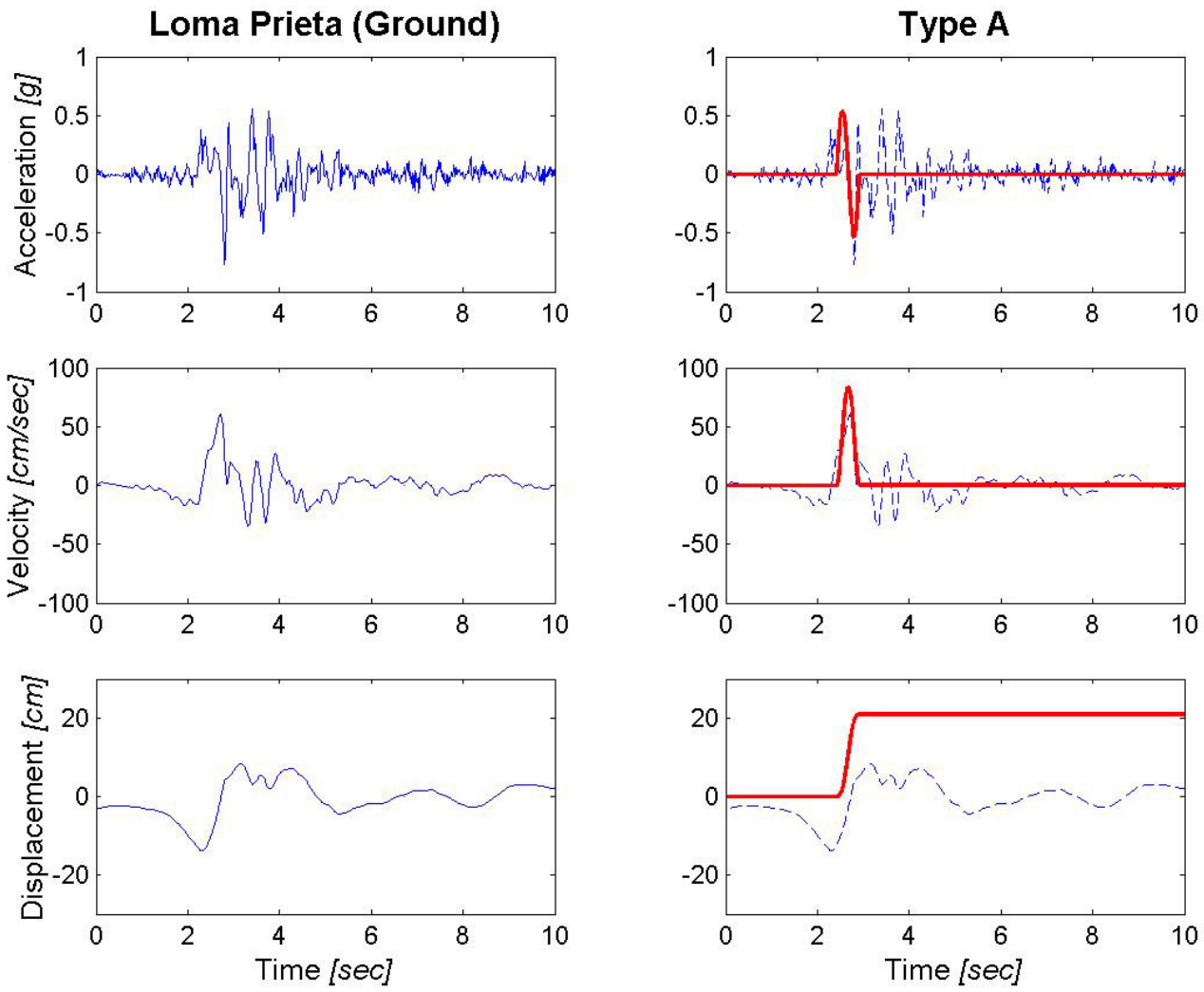

Figure A-5: Acceleration, velocity and displacement time histories recorded of Loma Prieta (ground) earthquake (right) and relative pulse approximation (left)

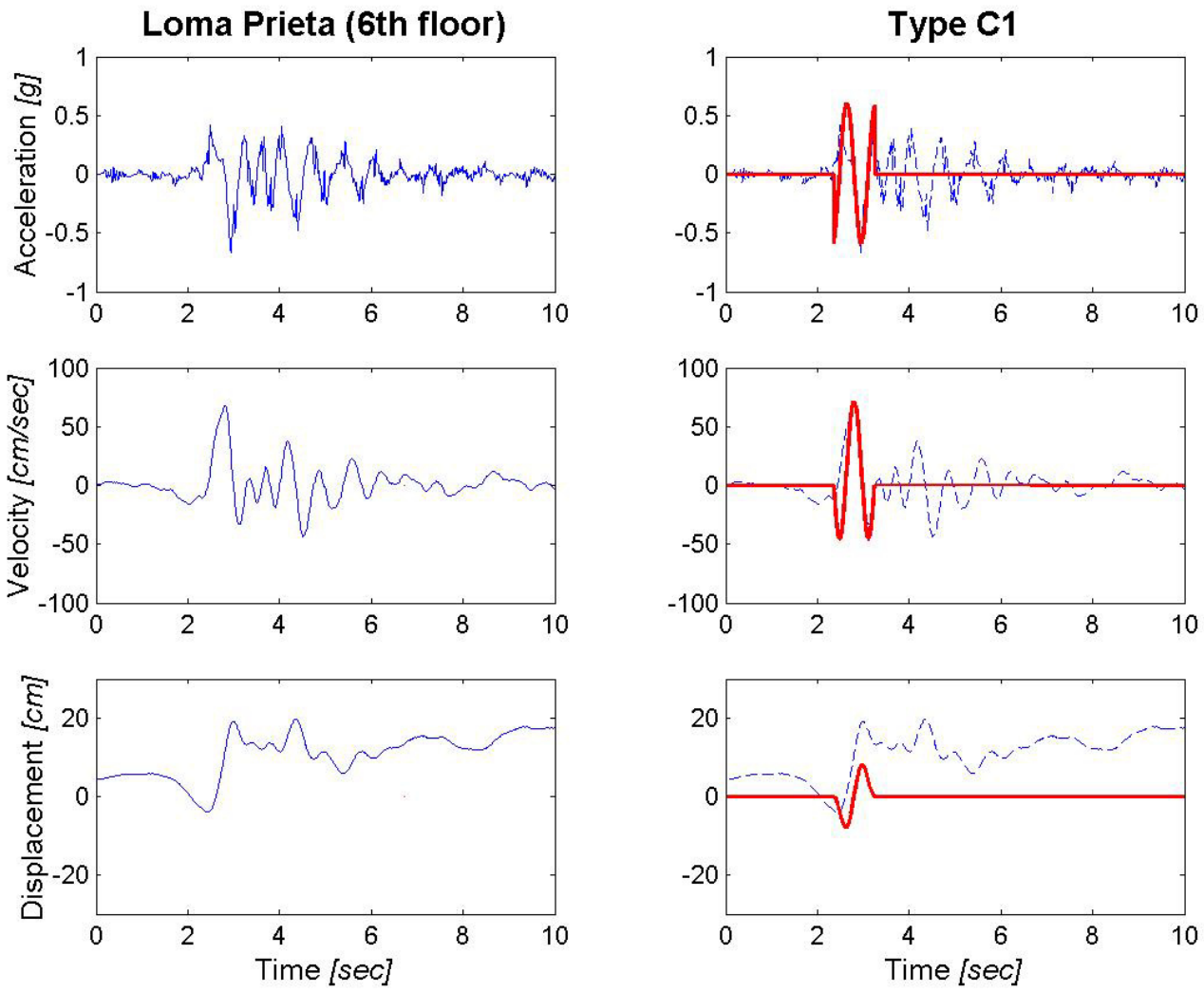

Figure A-6: Acceleration, velocity and displacement time histories recorded of Loma Prieta (6th floor) earthquake (right) and relative pulse approximation (left)

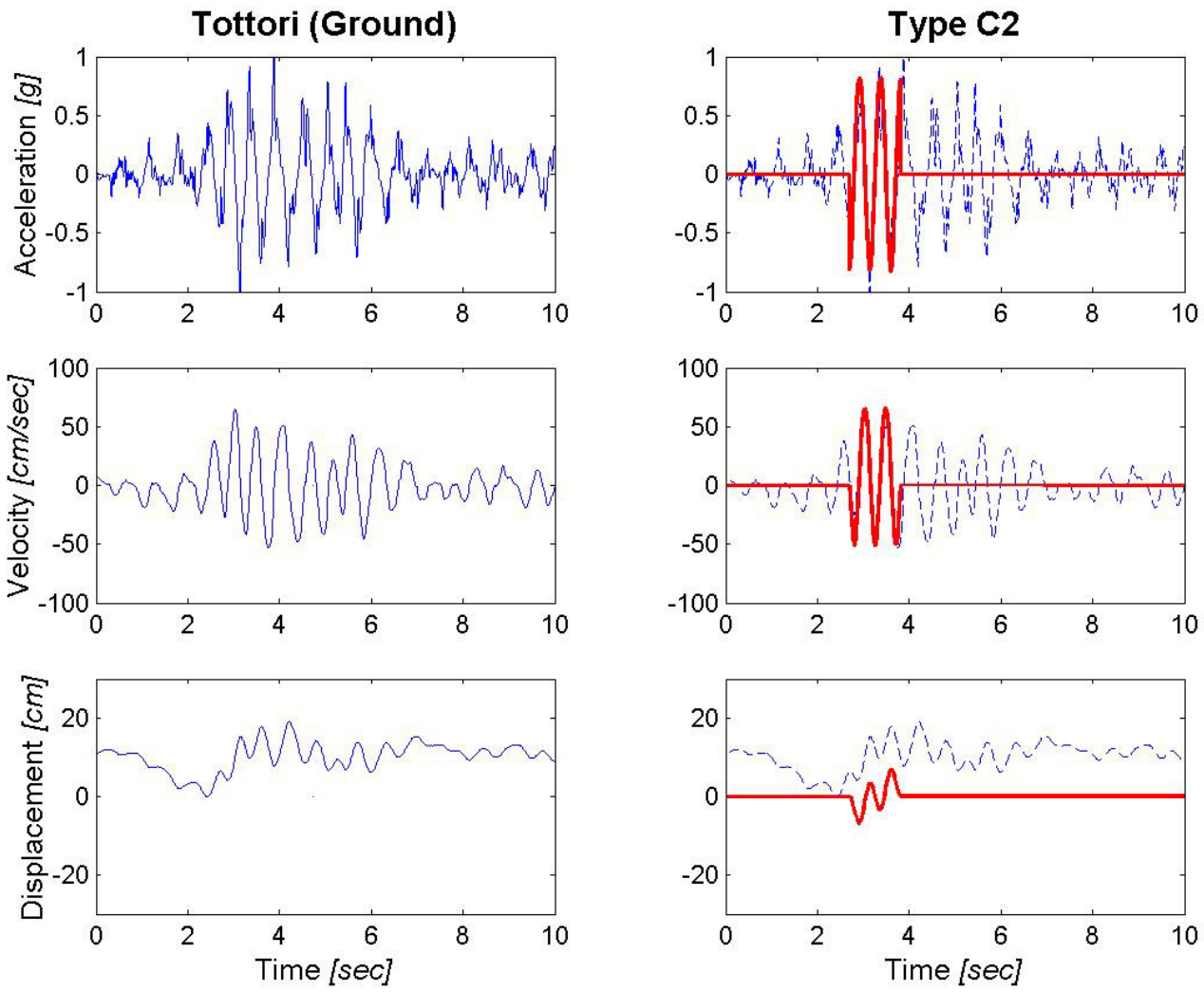

Figure A-7: Acceleration, velocity and displacement time histories recorded of Tottori (ground) earthquake (right) and relative pulse approximation (left)

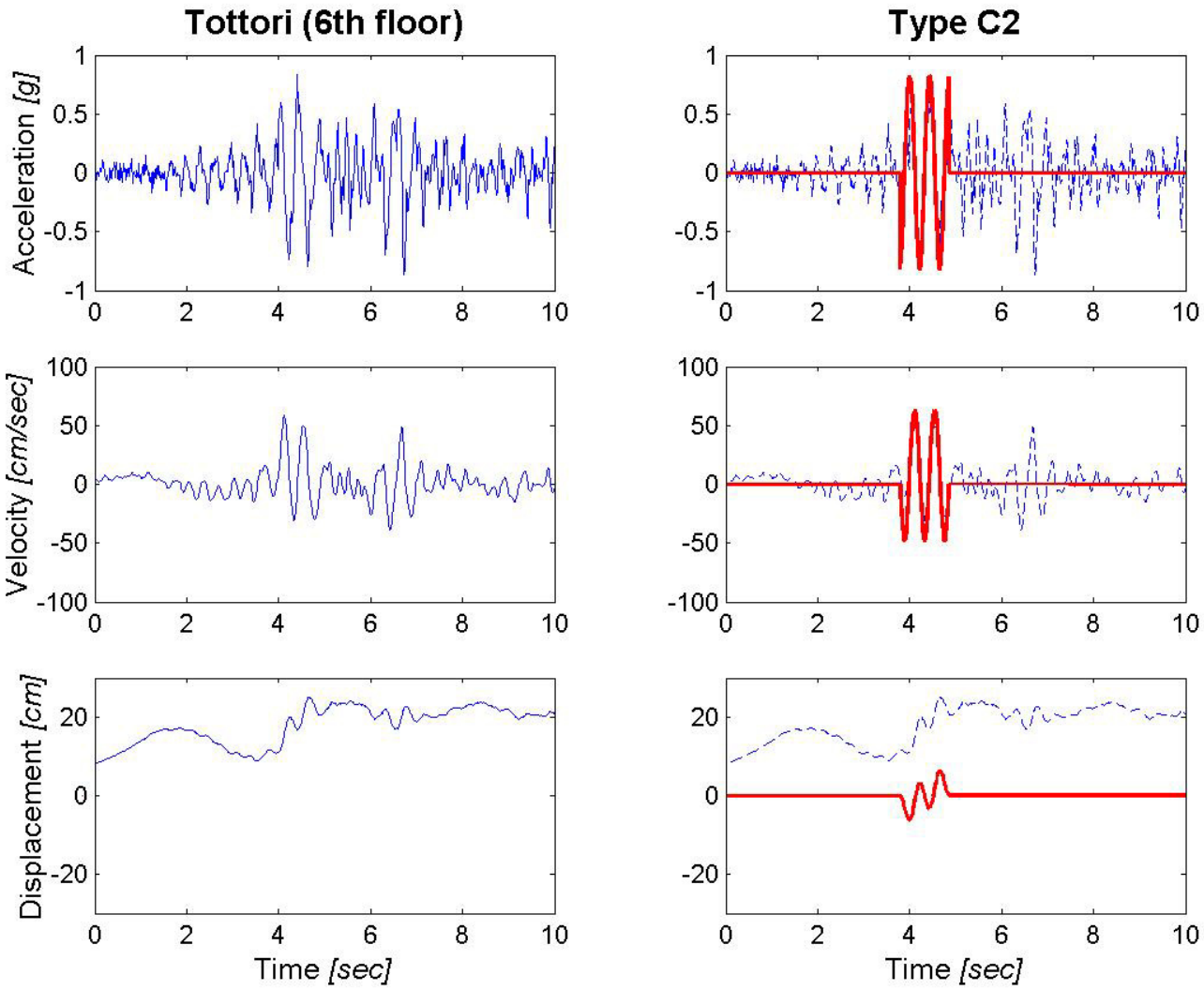

Figure A-8: Acceleration, velocity and displacement time histories recorded of Tottori (6th floor) earthquake (right) and relative pulse approximation (left)